

Key Points:

- White mica $^{40}\text{Ar}/^{39}\text{Ar}$ dating yields Paleogene ages in relic crenulations, while Miocene ages in the vicinity of shear zones
- Shear sense indicators imply top-NNW nappe stacking and top-W displacement along the Betic Movement Zone
- A new hypothesis is formulated for a gradual, Paleogene-early Miocene burial of the Nevado-Filábride Complex

Supporting Information:

Supporting Information may be found in the online version of this article.

Correspondence to:

K. Porkoláb,
kristof.porkolab@gmail.com

Citation:





Porkoláb, K., Matenco, L., Hupkes, J., Willingshofer, E., Wijbrans, J., van Schroyen Lantman, H., & van Hinsbergen, D. J. J. (2022). Tectonic evolution of the Nevado-Filábride Complex (Sierra de Los Filábres, southeastern Spain): Insights from new structural and geochronological data. *Tectonics*, 41, e2021TC006922. <https://doi.org/10.1029/2021TC006922>

Received 31 MAY 2021

Accepted 5 JUL 2022

© Wiley Periodicals LLC. The Authors. This is an open access article under the terms of the [Creative Commons Attribution License](#), which permits use, distribution and reproduction in any medium, provided the original work is properly cited.

Tectonic Evolution of the Nevado-Filábride Complex (Sierra de Los Filábres, Southeastern Spain): Insights From New Structural and Geochronological Data

Kristóf Porkoláb^{1,2} , Liviu Matenco¹ , Jasper Hupkes¹, Ernst Willingshofer¹, Jan Wijbrans³ , Hugo van Schroyen Lantman^{1,4}, and Douwe J. J. van Hinsbergen¹ 

¹Department of Earth Sciences, Utrecht University, Utrecht, The Netherlands, ²Institute of Earth Physics and Space Science (ELKH EPSS), Sopron, Hungary, ³Department of Earth Sciences, VU University Amsterdam, Amsterdam, The Netherlands, ⁴Njord Centre, Department of Geosciences, University of Oslo, Oslo, Norway

Abstract The high-pressure metamorphic Nevado-Filábride Complex (NFC) in the Betics mountain range of southeastern Spain exhibits continental and ocean-derived tectonic units, which are key for understanding the geodynamic evolution of the Western Mediterranean. We address the current debate in the definition of tectonic units, the emplacement of (ultra)mafic rocks, and the timing of burial metamorphism by conducting a structural study combined with single grain fusion $^{40}\text{Ar}/^{39}\text{Ar}$ dating of white micas in structurally critical outcrops of the eastern Sierra de Los Filábres. One older $^{40}\text{Ar}/^{39}\text{Ar}$ age population (38–27 Ma) is found at distance from the main shear zones in the relics of an early foliation, while a younger $^{40}\text{Ar}/^{39}\text{Ar}$ population (22–12 Ma) is dominant in the vicinity of these shear zones, where the early foliation is obliterated. Both age groups are interpreted as the record of deformation or fluid-induced recrystallization during distinct fabric-forming events, while alternative scenarios are discussed. A key observation is the presence of an ophiolitic mélangé, which— together with new and published geochronological data—allows for a new tectonic hypothesis. This considers Paleogene subduction beneath a Jurassic oceanic lithosphere, followed by the continued subduction of NFC and overlying ophiolites below the Alpujárride Complex. Exhumation during westward slab roll-back led to the formation of an extensional detachment system that obliquely cut nappe contacts. Although the timing constraints for high pressure-low temperature (HP-LT) metamorphism in the NFC remain inconclusive, the new tectonic hypothesis provides a solution that can account for both Paleogene and Miocene ages of HP-LT metamorphism.

1. Introduction

The Betic-Rif orogen in the Western Mediterranean region (Figure 1a) has been instrumental for understanding the role of slab dynamics and continental subduction-exhumation processes (Booth-Rea et al., 2015; Jolivet et al., 2021; Platt, Allerton, et al., 2003; Spakman et al., 2018). In a simplified form, the orogen consists of an Eocene and younger metamorphosed nappe stack, derived mainly from subducted continental crust (the internal Betic-Rif or the Alboran zone), which was emplaced during Miocene times over an imbricated, mostly non-metamorphosed sedimentary cover of the Iberian and North African margins (the external Betic and external Rif zones), as well as over the Atlantic oceanic crust in the Gulf of Cadiz (e.g., Azañón et al., 1998; Balanyá & García-Dueñas, 1987; Martínez Martínez, 1986; Platt, Allerton, et al., 2003; van Hinsbergen et al., 2020). Tectonic reconstructions and seismic tomography images have shown that the burial and exhumation history was associated with 400–800 km of subduction, even though the Africa-Iberia absolute plate convergence was only 100–200 km since Eocene times (Booth-Rea et al., 2007; Faccenna et al., 2004; Jolivet & Faccenna, 2000; van Hinsbergen et al., 2014). The excess in the amount of subduction is interpreted to result from slab roll-back that included a significant amount of westward slab retreat, more or less orthogonal to the N-S convergence direction between Africa and Iberia (Lonergan & White, 1997; Rosenbaum et al., 2002). In this general framework, the original geometry of the subduction zone (dipping N-NW vs. SE) and the exact amount of slab roll-back are still debated, which has resulted in a number of different paleogeographic and geodynamic scenarios (e.g., Bessière et al., 2021; Faccenna et al., 2004; Handy et al., 2010; Pedrera et al., 2020; Romagny et al., 2020; van Hinsbergen et al., 2020; van Hinsbergen et al., 2014; Vergés & Fernández, 2012). This debate is ultimately rooted in different interpretations of the timing and direction of nappe stacking, metamorphism, and exhumation of the units in the internal Betic-Rif orogen, and particularly in the Nevado-Filábride Complex of the Betics (NFC, Figure 1b). The

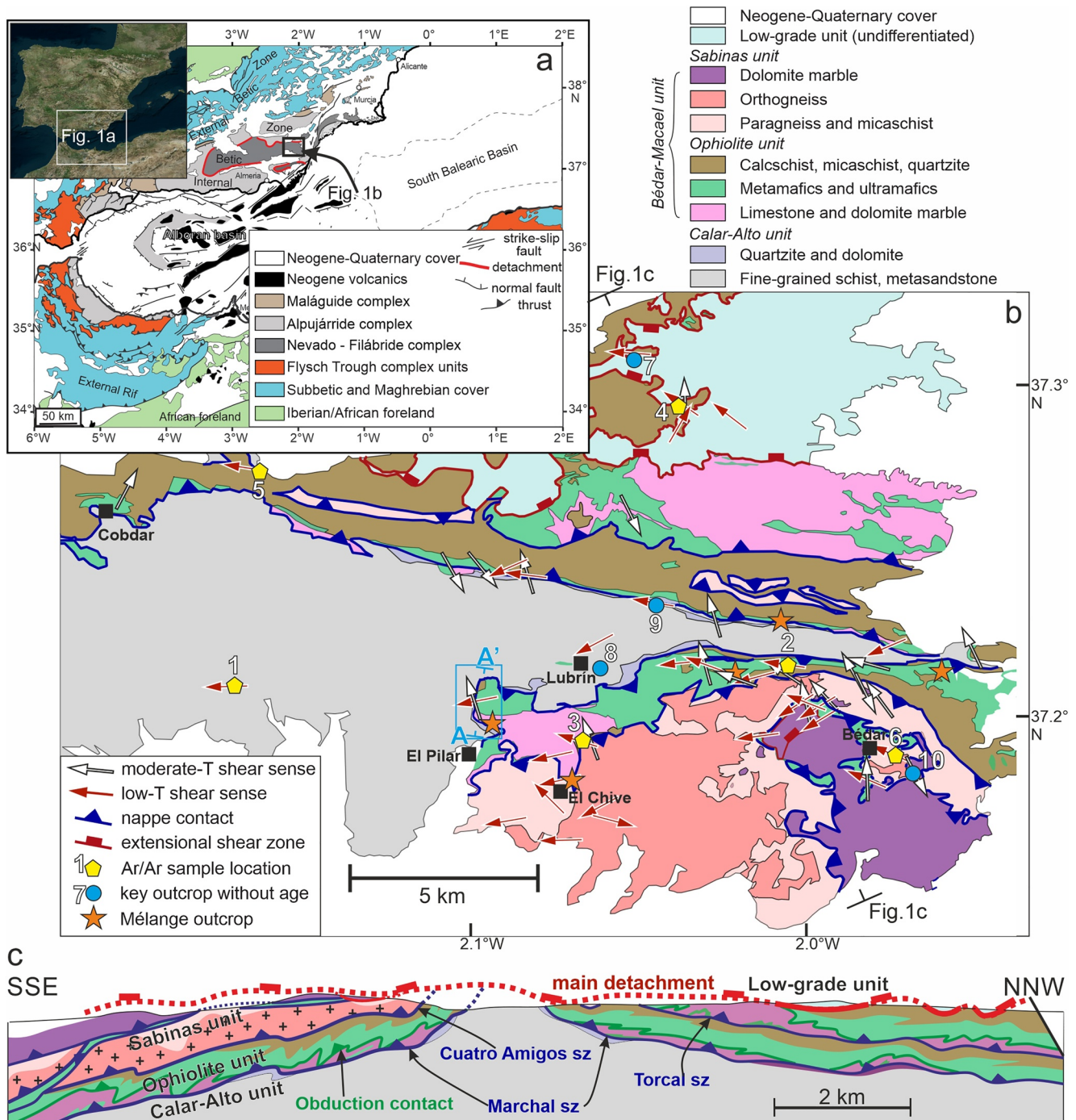


Figure 1. (a) Large-scale geological map of the Gibraltar arc (modified after Comas et al., 1999). (b) Geological map of the study area (eastern Sierra de Los Filábres), modified after Garcia Monzón et al. (1974), containing shear sense indicators, the locations of dating samples, and the location of other key outcrops. Plotted shear sense indicators are representative average values of numerous measurements per location (for the shear sense data see Table S1). A-A' is the location of the cross section on Figure 5a, presented together with a more detailed map of the cross section area (marked by blue box). (c) NNW-SSE cross section across the study area highlighting the major structural features (sz = shear zone).

NFC is a composite unit that contains both oceanic and continental rocks, metamorphosed up to eclogite-facies conditions. The eclogite-facies metamorphic fabric has yielded Eocene and Miocene geochronological ages, both interpreted as prograde metamorphism (Augier, Agard, et al., 2005; Kirchner et al., 2016; Li & Massonne, 2018; Monié et al., 1991; Platt et al., 2006; Sánchez-Vizcaíno et al., 2001). The NFC contains a (ultra)mafic unit, where

the presence of often metamorphosed Jurassic gabbros, dolerites, (pillow)basalts, pelagic sediments, and variously serpentinized peridotites implies a dominantly ocean-derived character (Puga et al., 2011, 1999). However, a number of observations such as the presence of depleted and serpentinized mantle rocks, Al-rich xenoliths in the metabasites, mafic dykes intruded into continental formations, and the analysis of detrital U-Pb zircon populations suggest that the rock succession might have originated from a hyper-extended continental margin setting (Gomez-Pugnaire & Munoz, 1991; Jabaloy-Sánchez et al., 2021; Laborda-López et al., 2020; Morten et al., 1987), similar to the the West Iberian Atlantic margin (e.g., Reston et al., 2007).

The NFC is truncated at the top by a major extensional detachment system (Betic Movement Zone or BMZ, Platt & Vissers, 1980; Martínez-Martínez et al., 2002) that separates it from the continental Alpujárride Complex (AC). The continental-derived AC was buried to high pressure-low temperature (HP-LT) metamorphic conditions in Eocene times (Azañón, 1997; Bessière, 2019; Bessière et al., 2022; Booth-Rea et al., 2002; Goffé et al., 1989; Monié et al., 1994; Platt et al., 2005) below rock units of the structurally highest, Maláguide Complex (MC). The AC and MC were interpreted to be derived from the AlKaPeCa microcontinental fragment that existed within the Alpine Tethys Ocean, together with tectonic units exposed in the Kabylides units of Northern Africa and units exposed on Sicily and Calabria (Bouillin et al., 1986; Handy et al., 2010; van Hinsbergen et al., 2014).

Two contrasting interpretations have been offered for the timing of burial in the NFC, based on different (or differently interpreted) geochronological data. One interpretation is based on Paleogene geochronological data derived from the continental units of the NFC in terms of $^{40}\text{Ar}/^{39}\text{Ar}$ ages on amphiboles (Monié et al., 1991) and white micas (Augier, Agard, et al., 2005; de Jong et al., 1992), and U-Th-Pb ages on monazites (Li & Massonne, 2018), interpreted as HP-LT metamorphism in the continental NFC falling into the range of ~48–30 Ma, simultaneously with the burial of the structurally higher AC (Bessière et al., 2022). This interpretation assumes Paleogene burial, while other Miocene geochronological ages are thought to reflect a stage of slow exhumation (e.g., Augier, Agard, et al., 2005; Bessière et al., 2021; Li & Massonne, 2018), resulting in a correlation of the NFC with the same paleogeographic continental unit as the AC and MC (AlKaPeCa unit, Bouillin et al., 1986). This interpretation is difficult to reconcile with the limited amount of Eocene convergence inferred by paleogeographic reconstructions (<100 km, e.g., van Hinsbergen et al., 2020), which appears to be insufficient for the burial of the entire oceanic to continental NFC domain.

Another interpretation is based on U-Pb zircon dating of mafic eclogites (Sánchez-Vizcaíno et al., 2001), Lu-Hf garnet dating of oceanic and continental rocks (Platt et al., 2006), and $^{87}\text{Rb}/^{86}\text{Sr}$ multi-mineral dating of one mafic eclogite and two metapelite samples (Kirchner et al., 2016), which yielded Miocene ages (~20–12 Ma). These ages are interpreted to reflect prograde burial metamorphism, which implies that the NFC belonged to the Iberian continental margin that subducted below the Alboran domain (AC and MC) during Miocene times. These studies however do not consider the Paleogene geochronological data reliable, and hence discard the interpretation of Paleogene NFC burial (e.g., Behr & Platt, 2012; Platt et al., 2006). Furthermore, a precise structural differentiation between nappe contacts and extensional detachments (BMZ) is still unclear across the NFC (e.g., Martínez-Martínez et al., 2002). The current NFC and AC definition in the key area exposing the (ultra) mafic unit (eastern Sierra de Los Filábres) follows the contrast in metamorphic grade, which was created by the tectonic omission along the BMZ after nappe stacking (Martínez-Martínez & Azañón, 1997; Martínez-Martínez et al., 2002; Platt & Vissers, 1980). Such a definition is difficult to be directly used for distinguishing paleogeographic domains stacked in a subduction zone.

In this study we aim to reconcile the tectonic architecture of the internal Betics in the key area of the eastern Sierra de Los Filábres, by focusing in particular on the juxtaposition of continental and ocean-derived units, together with the geometry, kinematics, and Ar/Ar age of shear zone foliations. We complement the extensive database of previous studies by kinematic mapping and structural analyses, together with single grain fusion $^{40}\text{Ar}/^{39}\text{Ar}$ dating of white micas in structurally strategic outcrops. We re-evaluate the kinematics and timing of tectonic burial in the NFC, allowing us to revisit the structural definition of tectonic units, constrain the paleogeographical and kinematic reconstructions of the Alboran region, and provide new insights on the mechanics of Cenozoic burial-exhumation processes.

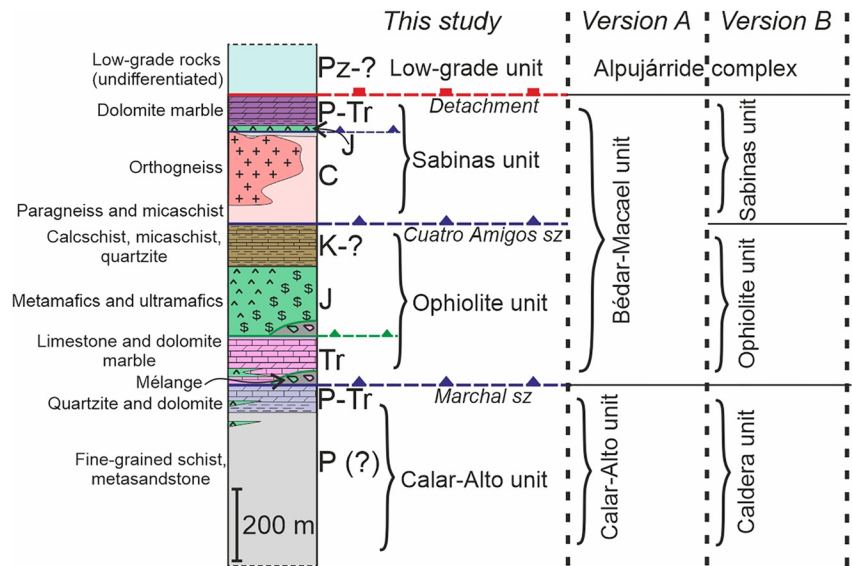


Figure 2. Tectono-stratigraphic column of the study area with the results of this study and the tectonic subdivisions used by previous studies, Version A (e.g., Booth-Rea et al., 2015; García-Dueñas et al., 1988; Martínez Martínez, 1984; Martínez-Martínez et al., 2002; Platt et al., 2006), and Version B (Puga et al., 2002, 2011, 2017).

2. Geological Setting

The internal Betic nappe stack consists of three major nappe complexes, from top to bottom the low-grade to non-metamorphic Maláguide (MC), the low-grade to high-grade Alpujárride (AC), and the medium to high-grade Nevado-Filábride (NFC) (e.g., Azañón, 1997; Balanyá & García-Dueñas, 1987; Booth-Rea et al., 2002; Martínez Martínez, 1984; Platt, Whitehouse, et al., 2003; van Hinsbergen et al., 2014; Vissers, 2012). The NFC is located in the core of an elongated, E-W oriented metamorphic dome system, while the AC and the MC make up the flanks of this structure (Figure 1a). In our study area of the eastern Sierra de Los Filábres (Figure 1b), only the AC and NFC are exposed.

The AC in the Eastern Sierra de Los Filábres consists of a Paleozoic succession of metapelites (phyllites) and quartzites, overlain by a Triassic succession of metamorphosed clastic sediments, evaporites (gypsum), carbonates, and mafic intrusive bodies (García Monzón et al., 1974). The AC is exposed on the northern flank of the eastern Sierra de Los Filábres and has been separated from the NFC largely based on its (locally) substantially lower metamorphic grade and on the presence of a regional-scale damage zone (e.g., Booth-Rea et al., 2002; García Monzón et al., 1974; Martínez-Martínez et al., 2002). The base of the AC is defined by a zone of retrograde mylonites and cataclasites that represent a major extensional detachment known as the BMZ, separating the AC in the hanging-wall from the NFC in the footwall across a significant tectonic omission (Martínez-Martínez et al., 2002; Platt et al., 1984; Platt & Vissers, 1980). The AC in the eastern Betics reached low-temperature blueschist facies metamorphic conditions with a peak temperature of 350–450°C (Booth-Rea et al., 2002) in Eocene times, interpreted as subduction-related metamorphism (Azañón, 1997; Bessièrre, 2019; Bessièrre et al., 2022; Goffé et al., 1989; Monié et al., 1994; Platt et al., 2005). Subduction of the AC was followed by its extensional exhumation reaching very low P/T gradients (within the andalusite stability field), resulting in a HT-LP metamorphic overprint during the early Miocene (Azañón et al., 1998; Booth-Rea et al., 2004; García-Dueñas et al., 1992; Lonergan & Johnson, 2002; Platt, Whitehouse, et al., 2003; Rossetti et al., 2005).

The NFC is defined as all rock units situated in the footwall of the Betic Movement Zone and is commonly subdivided into three tectonic units characterized by upward increasing metamorphic grade across the separating thrusts, while upward decreasing metamorphic grade within a single unit (Figure 2, Augier, Agard, et al., 2005; Augier, Booth-Rea, et al., 2005; Booth-Rea et al., 2015; Martínez Martínez, 1986; Martínez-Martínez et al., 2002). In the eastern Sierra de Los Filábres (Figure 1b), the Calar-Alto unit, equivalent of the Caldera unit (Puga et al., 2002), is composed of a thick (up to 1,500 m), likely Permian succession of medium to light-gray, pelitic schists (Tahal formation), underlain by the dark schists of the Montenegro formation, and overlain by

Permian to Triassic meta-conglomerates, quartzites, and carbonates, intercalated with small lenses of meta-mafic rocks (meta-dolerites) (Figures 1b and 1c, Figure 2, Garcia Monzón et al., 1974; Martínez Martínez, 1984, 1986). This unit is structurally overlain by the previously described (ultra)mafic unit thought to contain the remnants of a former oceanic lithosphere and those of a hyper-extended continental passive margin (Gomez-Pugnaire & Munoz, 1991; Laborda-López et al., 2020; Puga, 2005; Puga et al., 2011). The (ultra)mafic succession contains (meta)gabbros and dolerites, mantle peridotites of spinel-lherzolite composition and other, more or less depleted mantle rocks, such as cumulus troctolites, and are crosscut by doleritic and plagiogranitic dykes, which are best exposed in the area of Cobdar (Figure 1b, Puga, 2005). Furthermore, the same unit contains (meta)basalts showing preserved pillow and flow structures (Puga, 2005). The igneous age of the mafic rocks was determined by U-Pb dating of (meta-) gabbros and dolerites yielding Early Jurassic ages (185 ± 3 Ma, Puga et al., 2011). The (ultra)mafic succession is overlain by metasediments (quartzites, micaschists, and calcschists), interpreted to be part of a pelagic sequence that formed on the ocean floor possibly during Cretaceous time (Puga et al., 2011; Tendero et al., 1993).

The structural separation of the (ultra)mafic unit is debated. One group of studies include these rocks in a Bédar-Macael unit that also contains Paleozoic and Mesozoic continental formations (version A on Figure 2, e.g., Augier, Agard, et al., 2005; Martínez Martínez, 1984; Martínez-Martínez et al., 2002; Platt et al., 2006). The observation of small mafic bodies and dykes intruding the continental formations of the Calar-Alto unit and the overlying carbonates (Booth-Rea et al., 2009a, 2009b; Morten et al., 1987), U-Pb age populations of detrital zircons (Jabaloy-Sánchez et al., 2018, 2021), and stratigraphic studies (Ortí et al., 2017; Simon, 1987) support the common origin of a mixed continental-oceanic NFC succession, interpreted to be derived from a former hyper-extended continental margin (Booth-Rea et al., 2015; Gomez-Pugnaire & Munoz, 1991; Laborda-López et al., 2020). This interpretation does not account for the observations that the (ultra)mafic rock sequence contains all the elements of a typical (although dismembered and metamorphosed) oceanic lithosphere sheet, favored by the second group of studies defining a separate Ophiolite unit (version B on Figure 2, Puga et al., 2002, 2011). Regardless the structural definition, the (ultra)mafic unit is interpreted by geophysical studies to have a significantly larger thickness (4–9 km) at depth, beneath Sierra de Los Filábres (Pedrera et al., 2009). However, the structural position and significance of this deep (ultra)mafic body is unclear.

An interesting structural situation is the contact between the (ultra)mafic unit and the overlying sequence, best exposed in the area of Bédar (Figure 1b). Here, the (ultra)mafic unit and associated metasediments are overlain by a large Carboniferous orthogneiss (meta-granite) body (Martínez-Martínez et al., 2010), which is intruded into metasediments (paragneisses and micaschists) of possibly pre-Carboniferous age, interpreted to be part of the same Bédar-Macael unit (version A on Figure 2, García-Dueñas et al., 1988; Martínez-Martínez et al., 2002, 2010) or in a different Sabinas unit (version B on Figure 2, Puga et al., 2002, 2011). The contact between the Carboniferous and underlying Jurassic (-Cretaceous?) rocks (Figure 2) is interpreted to be either a thrust (Puga et al., 2002) or the result of a large-scale recumbent fold with the orthogneiss in its core (García-Dueñas et al., 1988; Martínez-Martínez et al., 2002, 2010). This controversy is just apparent, since a recumbent fold must be sheared along the overturned flank to explain the very rapid change in age, which results in a fold nappe type of thrusting geometry.

2.1. Metamorphic Conditions and Kinematic Characteristics of the NFC

The Calar-Alto unit (Figure 2) reached eclogite-grade peak burial metamorphic conditions in the order of 14 kbar/550°C (Augier, Agard, et al., 2005), 20–22 kbar/470–490°C (Santamaría-López et al., 2019), or 16.2–18.6 kbar/519–543°C (Li & Massonne, 2018). In the thick, dominantly metapelitic formation, the HP-LT mineral paragenesis consists of garnet, chloritoid, phengite, chlorite, kyanite, and rutile (e.g., Augier, Agard, et al., 2005; Booth-Rea et al., 2015). The micaschists and orthogneiss bodies of the Sabinas unit reached similar or slightly higher eclogite-grade peak burial conditions with thermodynamic estimations of 20 kbar/520°C (Santamaría-López et al., 2019), or 20–22 kbar/550–600°C (Ruiz-Cruz et al., 2015). The (ultra)mafic unit (Figure 2) reached similar eclogite-grade peak metamorphic conditions, developing a mineral paragenesis consisting largely of omphacite, garnet, and phengite in the meta-mafic rocks (e.g., Puga et al., 1999). Thermodynamic estimates of peak metamorphic conditions for the mafic eclogites are in the range of 14–22 kbar/570–675°C (Puga et al., 2000), 16–17 kbar/680–710°C (Padrón-Navarta et al., 2010), 20–22 kbar/550–600°C (Ruiz-Cruz et al., 2015), 16–22 kbar/500–700°C (Augier, Agard, et al., 2005), or 17–19 kbar/680°C (Menzel et al., 2019).

Numerous studies have interpreted that both the continental and (ultra)mafic protoliths experienced an additional episode of heating during their decompression, that is, exhumation (Booth-Rea et al., 2015; Li & Massonne, 2018; Puga et al., 2000; Santamaría-López et al., 2019), although retrograde P-T paths implying isothermal decompression (Augier, Agard, et al., 2005) or cooling during decompression (e.g., Behr & Platt, 2012) have also been reported. Retrograde metamorphism in the metapelites of the Calar-Alto and Bédar-Macael units is characterized by the abundant growth or recrystallisation of chlorite, albite, white mica, and quartz, which define the post-HP tectonic foliation(s) (Augier, Agard, et al., 2005; Booth-Rea et al., 2015). Following medium-to low-temperature retrograde metamorphism, the NFC experienced significant further cooling and exhumation to (or near) the surface during the late Miocene (Agard et al., 2011; Augier et al., 2013; Johnson, 1997; Lonergan & Johnson, 2002; Vázquez et al., 2011).

The kinematics of deformation during HP-LT metamorphism in the NFC is largely unknown due to the significant amount of obliteration during the subsequent moderate-to low-temperature shearing (e.g., Augier, Agard, et al., 2005). Retrograde mineral assemblages in the NFC overgrow a relic S_0 sedimentary layering and the early, HP-LT, S_1 tectonic foliation, which is preserved in the deeper sections of the Calar-Alto unit, and is progressively obliterated toward the Marchal shear zone (García-Dueñas et al., 1988), where the S_2 or younger foliations become more closely spaced (Augier, Agard, et al., 2005; Booth-Rea et al., 2015). The pervasive $S_{2(-3)}$ foliation(s) carries stretching lineations that are dominantly associated with a top-W sense of shear during exhumation, especially close to the main extensional detachment system (BMZ, Augier, Agard, et al., 2005; Booth-Rea et al., 2015; Martínez-Martínez et al., 2002; Platt & Vissers, 1980). Augier, Jolivet, and Robin (2005) furthermore reported the divergence of this generally westward shear direction on either limbs of the NFC dome. Retrograde shearing in the formations of the NFC finally transitioned to cataclastic to brittle shearing and normal faulting along the Betic Movement Zone (Augier, Jolivet, & Robin, 2005; Martínez-Martínez et al., 2002).

3. Structural and Tectono-Stratigraphic Results

We complement the extensive available kinematic database by conducting a fieldwork with the aim of detailing the geometry, kinematics, and metamorphic conditions of the main shear zones as well as making new observations regarding the present structural relationship between the original continental and (ultra)mafic protoliths. We build on the already established petrological data and use further field and microstructural criteria to infer the kinematics of shearing during the established metamorphic stages. We used stretching lineations and associated kinematic indicators such as shear bands (C-S or C'-S structures, Figures 3c and 4f), or asymmetric porphyroclasts (Simpson & Schmid, 1983) to infer tectonic transport directions under different metamorphic conditions. The measured stretching lineations can be generally grouped in two categories based on minerals that are characteristic for metamorphic facies: moderate-temperature (developed around 450°C), representing post-peak metamorphic conditions prevailing during deep burial and early exhumation (e.g., Booth-Rea et al., 2015), and low-temperature, representing the retrograde metamorphic stage during significant decompression (exhumation) in the NFC (Figures 1b and 3a, e.g., Augier, Agard, et al., 2005). Moderate-temperature stretching lineations are usually defined by black and blue amphiboles and plagioclase in the metamafic rocks. Low-temperature stretching lineations are defined when arguments for retrograde mineral growth with respect to moderate-temperature conditions were found in the field or thin sections. These are situations when: (a) low-grade minerals, most frequently chlorite and albite (Augier, Agard, et al., 2005) overgrow higher-grade fabrics with no moderate-temperature lineation preserved (see also Augier, Agard, et al., 2005); (b) a moderate-temperature stretching lineation is still preserved, but it is overprinted by retrograde lineations while keeping the same sense of shear; (c) a moderate-temperature stretching lineation is still preserved in some foliation planes, but a second set of stretching lineations overprint the first set with a different orientation, defined by different minerals, such as chlorite, albite, green amphibole, white mica, quartz or calcite.

3.1. Kinematics of Deformation

A large part of our structural observations are similar to those of previous studies in terms of foliations, superposition of folding and shearing characteristics (e.g., Augier, Agard, et al., 2005; Booth-Rea et al., 2015; Martínez-Martínez et al., 2002). Therefore, we avoid an extensive repetitive description and focus on new kinematic observations that are herewith described in more detail.

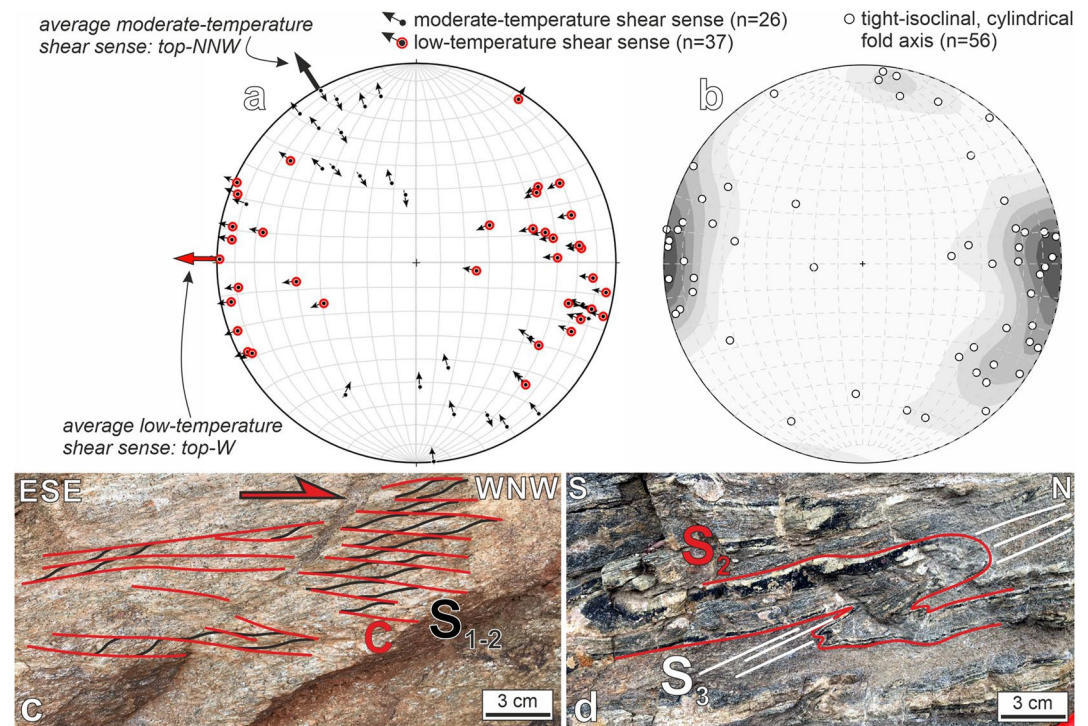


Figure 3. (a) Stereographic projection of moderate and low-temperature stretching lineations and associated kinematic indicators. Plotted shear sense indicators are representative average values of numerous measurements per location. (b) Stereographic projection of cylindrical, asymmetric, tight-isoclinal fold axes ($F_{2,3}$). (c) C-S shear fabric in garnet-micaschist at the top of the Ophiolite unit (Cuatro Amigos shear zone) showing top-WNW sense of shear. (d) Tight, asymmetric, N-verging fold (F_3) in mafic amphibolite showing the crystal-plastic deformation (flow) of plagioclase.

The NFC in the eastern Sierra de Los Filábres displays a gradual change of ductile structural elements from the core of the dome (deeper sections of the Calar-Alto unit) toward its flanks, where the Marchal and Cuatro Amigos shear zones crop out (Figures 1b and 1c). The metapelites in the core of the dome show a distinct succession of folds and related axial planar cleavages that are largely obliterated by the development of shear zone foliation in the proximity of these shear zones. A generation of early isoclinal folds (F_1) is only observed in the metapelites of the Calar-Alto unit. These folds affect the S_0 sedimentary layering, are generally rootless and transposed into the tectonic foliation of the subsequent folds (S_2 , Figures 4a and 4c). F_2 isoclinal folds are associated with a pervasive S_2 foliation. The S_0 , S_1 and S_2 foliations are generally (sub-)parallel in the areas close to the shear zones (composite $S_{0,2}$ foliation, Figures 4b and 4f), while in the deeper sections of the Calar-Alto unit S_2 foliation defines a strong crenulation cleavage in the meta-pelitic rocks (Figures 4a and 4c). Tight to isoclinal, dominantly asymmetric folds (F_3) refold the pervasive S_2 foliation and F_2 isoclinal folds, associated with an occasionally strongly developed S_3 tectonic foliation (Figure 3d). In the shear zones, the tight F_3 asymmetric folds are flattened to isoclinal fold geometries and the S_3 foliation becomes sub-parallel to the S_2 foliation, making their distinction difficult in places. These two generations of tight-isoclinal, cylindrical folds ($F_{2,3}$) were measured in all exposed units of the NFC in our study area and show dominant E-W oriented fold axes (Figure 3b), and gently dipping ($<45^\circ$) axial planes. These folds are dominantly asymmetric and have a \sim N-ward vergence (e.g., Figures 1c and 3d). The exception is the El Pilar–El Chive area, where consistent southward vergence of asymmetric F_3 folds is observed in the meta-mafic and carbonate rocks (Figures 4a and 4d). $F_{2,3}$ folds are the product of ductile deformation (flow) and show oriented growth of plagioclase and black to blue amphiboles in the meta-mafic rocks, implying that the formation of these folds was coeval with moderate-temperature shearing that followed peak metamorphism (Figure 3d). S_2 and subordinately S_3 foliation planes carry well-developed stretching lineations. Based on field and micro-structural observations, two generations of stretching lineations can be distinguished. Moderate-temperature stretching lineations and coupled kinematic indicators show an average top-NNW (top- 330°) sense of shear, while low-temperature stretching lineations (including a transition from moderate to low-temperature while keeping the same sense of shear) show an average top-W (top- 271°) sense

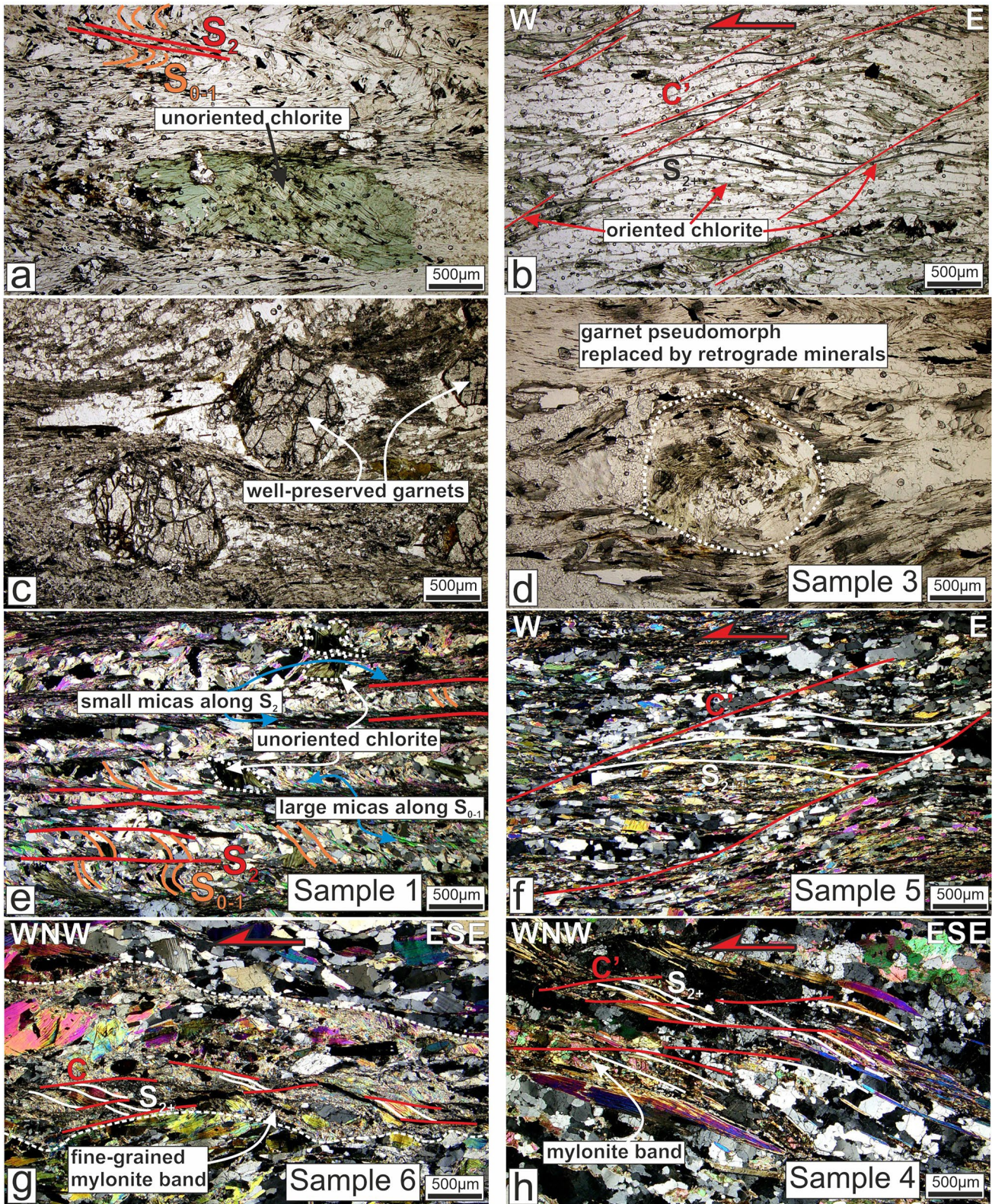


Figure 4.

of shear (Figure 3a). The more northerly directed tectonic transport during moderate-temperature metamorphic conditions is in agreement with the dominantly E-W trending and N-verging, cylindrical, asymmetric $F_{2,3}$ folds (Figures 3a and 3b, also described by Augier, Jolivet, & Robin, 2005). Summarizing the kinematic observations, moderate-temperature shearing occurred dominantly toward the NNW, and shifted toward the W during lower-temperature retrograde shearing.

3.2. Shear Zones and Tectonic Units in the Eastern Sierra de Los Filábres

The mapping of the main shear zones, complemented with new observations regarding the tectono-stratigraphic superposition of the formations, has led to a refinement of the commonly used subdivision of tectonic units for the eastern Sierra de Los Filábres (Figures 1c and 2). The base of the Calar-Alto unit is not exposed in our study area. The top of this unit is defined by the Marchal shear zone (García-Dueñas et al., 1988). This shear zone is often observed in mylonitic quartzites and marbles situated in the uppermost part of the Calar-Alto unit or in the marbles and amphibolites in the lower part of the Ophiolite unit (Figures 1c and 2). The shear zone shows NW-SE to E-W oriented stretching lineations and associated top-NW to W sense of shear (Figure 4b). Along the northern flank of the Sierra de Los Filábres, a repetition of the Ophiolite unit is observed (Figures 1b and 1c). This repetition is explained by a reverse-sense shear zone (herewith named Torcal shear zone), which does not exhibit consistent shear sense directions (both top-E and top-W kinematic indicators). The top of the Ophiolite unit is marked by the basal shear zone of the Sabinas unit, herewith named the Cuatro Amigos shear zone, which is observed in the amphibolites, micaschists, and calcschists of the Ophiolite unit, and in the Carboniferous orthogneiss of the Sabinas unit. The shear zone exhibit mylonites and ultramylonites, where the observed stretching lineations are dominantly retrograde, trending WNW-ESE associated with a top-WNW sense of shear, as observed, for instance by a well-developed C-S fabric in the micaschists of the Ophiolite unit (Figure 3c). Given that the significantly older Carboniferous orthogneiss tectonically overlies the Ophiolite unit, we describe it as an initial thrusting contact between the Ophiolite and Sabinas units (the Cuatro Amigos shear zone, Figure 2). This is not incompatible with the fold-nappe solution described in detail by García-Dueñas et al. (1988), with the exception that the overturned flank of the fold-nappe must have accommodated larger amounts of thrusting (shearing) than hitherto assumed. The Sabinas unit is further dissected by multiple shear zones causing a complex repetition of formations including a thin sliver of mafic amphibolites and serpentinites outcropping below Triassic dolomite marbles (Figure 1c).

3.2.1. Lithostratigraphy and Structure of the Ophiolite Unit

Starting from the lithological composition and the mafic-ultramafic petrography of the Ophiolite unit extensively described by previous studies (e.g., Puga et al., 1999, 2000, 2011), our observations show that the base of this unit generally displays Triassic meta-carbonates (dominantly calcite marbles and subordinately dolomite marbles) folded together with thin layers of meta-mafic rocks (Figures 5a and 5c). The meta-carbonates are in most sections overlain by the Jurassic mafic and ultramafic rock succession that can reach a thickness of 250 m. (Meta-)mafic rocks are dominantly fine to coarse grained amphibolites, often containing relics with the texture of the basaltic, doleritic, or gabbroic protoliths. The amphibolites are characterized by a clearly developed, often mylonitic foliation defined by stretched plagioclase and oriented amphibole crystals. The mineralogical association of the amphibolites often includes epidote and garnet, which appear to be pre- to syn-kinematic with respect to deformation in the main shear zones. Other rocks observed are large bodies of serpentinites, locally reaching a thickness of 150 m (Figure 5h), serpentinite-schists (for details also see Menzel et al., 2019), and talc-schists. The serpentinite schists generally show well-developed $S_{2,3}$ foliations that are continuous with the ones in the

Figure 4. Interpreted thin section pictures showing the microstructure of geochronologically dated and other key samples. The sample location is plotted on Figure 1b. (a) Plain polarized thin section picture of the Tahal formation, outside of the Marchal shear zone (Key outcrop 8 on Figure 1b), showing unoriented chlorite growth during retrogression and the preservation of an early $S_{0,1}$ foliation in relic crenulations. (b) Plain polarized thin section picture of the Tahal formation, inside the Marchal shear zone (Key outcrop 9 on Figure 1b), showing oriented chlorite growth. Older fabrics (S_0 , S_1 , possibly S_2) are completely overprinted by the shear zone foliation. C'-type shear bands imply top-W sense of shear. (c) Plain polarized thin section image of well-preserved garnet porphyroclasts in the Sabinas unit (Key outcrop 10 on Figure 1b) outside of the main shear zones. (d) Plain polarized thin section picture of a garnet pseudomorph within the Cuatro Amigos shear zone, largely replaced by white mica and quartz (Sample three on Figure 1b). (e) Cross-polarized picture of Sample 1 showing the preservation of the early $S_{0,1}$ foliation in crenulations and the unoriented growth of chlorite. Large mica crystals define the $S_{0,1}$ foliation, while small micas define the S_2 foliation. (f) Cross-polarized picture of Sample 5 showing a mylonitic foliation and top-W C'-type shear bands. (g) Cross-polarized picture of Sample 6 showing a band of fine-grained mylonite associated with top-WNW sense of shear in the orthogneiss of the Sabinas unit. (h) Cross-polarized picture of Sample 4 showing mylonite bands associated with top-WNW sense of shear directly below the BMZ.

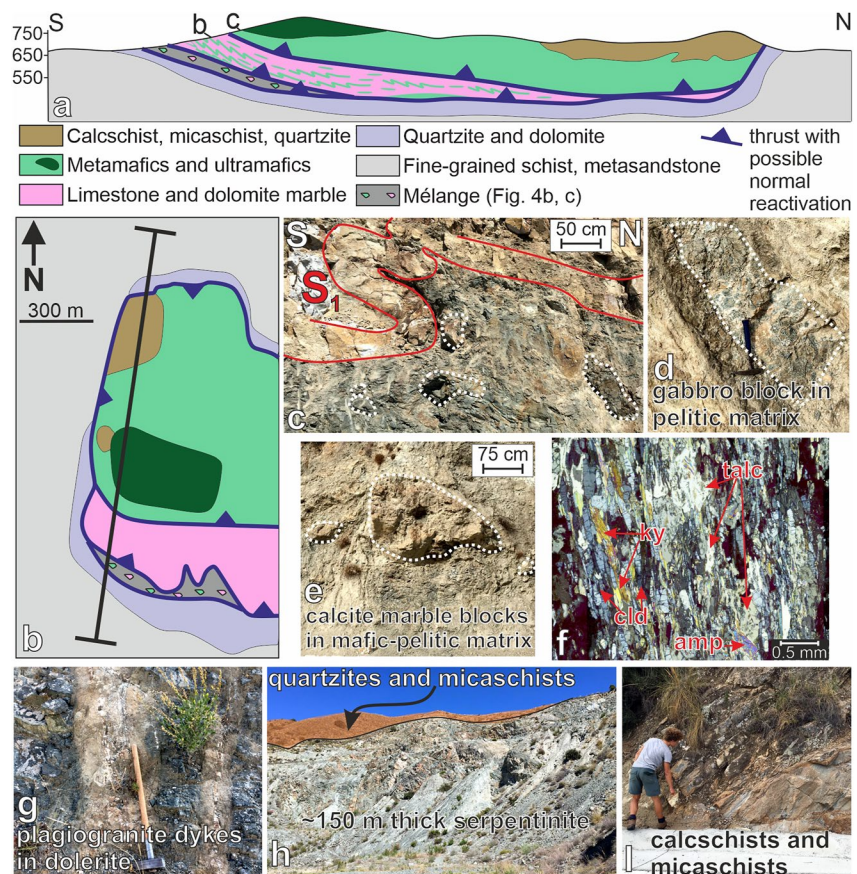


Figure 5. Structure and composition of the Ophiolite unit. (a) Cross section through the ophiolite unit at the El Pilar location (for map-view trace of the section see subplot (b) on this figure, and Figure 1b). Note the consistent southward vergence of asymmetric folds that affect thin slivers of metamafics and the metacarbonates together. (b) Geological map detail showing the area of the cross section. (c) SSW-verging asymmetric fold in shallow-water carbonates (limestone marble). The carbonate layer is underlain by fine-grained mafic amphibolite displaying several mafic blocks of similar composition. (d) (Meta) Gabbro block in pelitic matrix in the mélangé formation of the Ophiolite unit. See hammer for scale. (e) Calcite marble block in mafic-pelitic matrix in the mélangé of the Ophiolite unit. (f) Interpreted thin-section picture of a chloritoid-talc-kyanite schist sample taken from the metamorphosed ophiolitic mélangé. The association between chloritoid (cld), amphibole (amp), talc, kyanite (ky), white mica, quartz, and plagioclase indicate a mixed sedimentary-altered mafic protolith affected by high-pressure metamorphism. (g) Plagiogranite dykes in dolerite at Cobdar. (h) Thick body of serpentinite covered by quartzites and micaschists. (i) Calcschists and micaschists that cover the mafic and ultramafic formations of the Ophiolite unit.

surrounding rocks. In the Cobdar area (Figure 1b), previous studies have described extensively the structure, composition, and petrography of mantle rocks, such as peridotites or cumulus troctolites, affected by a significant degree of metasomatism and alteration from serpentinites to talc, together with gabbros, dolerites, and pillow basalts (e.g., Puga et al., 1999, 2011, 2017). The crustal rocks are cut by numerous dykes of (porphyric) basalts, dolerites, and plagiogranites (or plagiogneisses when metamorphosed) that locally retain the typical sheeted-dykes geometry or composition (Figure 5g). The mafic and ultramafic rocks are overlain by calcschists, garnet-micaschists, and quartzites, interpreted to represent a syn- to post-rift deep-water successions deposited on top of the oceanic rocks (Figures 5a, 5b, 5h and 5i, Puga et al., 2011; Tandero et al., 1993). These metasediments cover both the mafic and ultramafic rocks of the Ophiolite unit (Figures 5a and 5b). The different lithologies of the Ophiolite unit display various vertical superpositions of different rock types due to the effect of several successive deformation phases and is significantly omitted in or near the vicinity with the BMZ or associated exhumation shear zones.

One key observation not described previously is that the (meta)mafic, ultramafic, and (meta)sedimentary formations of the Ophiolite unit are often mixed in a mélangé that often still preserves the olistostrome structure of

the original protolith, despite the superimposed shearing and metamorphism (Figures 5a and 5b). The *mélange* is made up largely by a talc, serpentinite, or meta-siltic and pelitic matrix (Figure 5f), surrounding centimeters to tens of meters sized (meta)sedimentary and (meta)mafic blocks, such as calcite or dolomite marbles (e.g., Figure 5e), quartzites, various types of schists, metamorphosed basalt, dolerite, gabbro (e.g., Figure 5d), or meta-conglomerates. The (meta)mafic blocks often preserve the original gabbroic, doleritic, or basaltic texture (e.g., Figure 5d) and the surrounding matrix is typically rich in talc (Figure 5f), serpentinite, and meta-mafic minerals, mixed with meta-sedimentary blocks or matrix, sometimes including secondary gypsum. Thin section analysis shows the dominance of chloritoid, talc, kyanite, and amphiboles in the fine-grained *mélange* matrix (Figure 5f). The proportion of mafic and siliciclastic material is highly variable within the *mélange*. The S_{2-3} foliation is independent of the contacts between different lithologies within the *mélange*, generally crosscutting throughout the matrix and blocks of various composition, suggesting that the formation of the *mélange* predate the D_2 tectono-metamorphic event. The best preserved section (from El Pilar toward Lubrin along the main road) displays a typical ophiolitic *mélange* facies, with mafic blocks mixed together with other blocks of meta-sediments, enclosed in a talc- and serpentinite-rich sedimentary matrix (Figures 5a, 5b, 5d and 5e). The *mélange* is cut by a series of dominantly NW-dipping, late normal faults, but still retains the original olistostrome structure (Figures 5a, 5b, 5d and 5e). The *mélange* formation outcrops at numerous locations in the eastern Sierra de Los Filábres (Figure 1b), and exhibit various grades of metamorphism and style of deformation. The deformation observed in the Ophiolite unit is mostly similar with the one observed in all other units. The exception is the area of the El Pilar and El Chive (Figure 1b), where the meta-mafic and ultramafic rocks and the ophiolitic *mélange* are better exposed and preserved. In this area, a generation of asymmetric folds has been observed, which have a consistent top-SSW vergence (Figures 5a and 5c), in contrast to the typical N-ward vergence of F_{2-3} asymmetric folds observed elsewhere.

3.2.2. Additional Tectono-Stratigraphic Observations in the Low-Grade Unit

Along the northern flank of the Sierra de Los Filábres, a tectonic omission creates a significant offset from high-grade to low-grade metamorphic conditions (the low-grade unit in this area commonly interpreted as the AC, e.g., Augier, Agard, et al., 2005; Booth-Rea et al., 2015; Martínez-Martínez et al., 2002), separated by a zone containing originally high-grade rocks that were retrogressed during mylonitization and cataclasis (faulting), which mark the previously mapped BMZ of Platt and Vissers (1980). The retrogressed mylonites in the footwall largely consist of garnet-micaschists that overlie the mafic and ultramafic rocks of the Ophiolite unit (Figure 6a). These garnet-micaschists are characterized by the retrograde growth of chlorite, calcite, and quartz at the expense of the peak metamorphic mineral assemblage (Figure 6b). Stretching lineations carried by chlorite are associated with clear top-W shear sense indicators. The retrograde mylonites are often reworked as cataclasites and cut by numerous normal faults that post-date the cataclastic foliation (Figure 6c). The transport direction of the cataclastic shear bands and normal faults are also top-W, in agreement with the ductile kinematic indicators in the retrograde mylonites (Figure 6c).

In the hanging-wall of the BMZ, the low-grade formations show significant lithological similarity to the underlying formations of the NFC. The basal formation of the low-grade unit consists of thick successions of metapelites and quartzites that are the low-grade equivalents of the Permian strata of the Calar-Alto unit. The metapelites only show the grade of phyllitic cleavage in terms of fabric development, while the quartzites developed a less closely spaced tectonic foliation compared to those of the Calar-Alto unit. In some sections, the BMZ is directly overlain by non-metamorphosed or very low-grade dolerites and basalts in the hangingwall that preserved their igneous textures and mineral composition (Figures 6d and 6e). These mafic rocks may correspond to a non-metamorphic equivalent of the Jurassic meta-mafic rocks (fine and coarse-grained amphibolites) in the Ophiolite unit located beneath the BMZ. These mafic rocks are also overlain by dolomites, which do not show a developed tectonic foliation or signs of metamorphic recrystallization, attesting to relatively low metamorphic facies (lower greenschist facies and below). The dolomites could be the protolith equivalents of the Triassic dolomite marbles observed in the NFC.

3.2.3. Strain Distribution During Exhumation (Retrograde Metamorphism)

Mapping of structural and metamorphic features with special attention to the superposition of moderate and low-temperature fabrics allowed us to delineate zones where strain localization during retrograde metamorphism took place in our study area. A large amount of deformation was accommodated along the BMZ extensional detachment system (around 110 km of extension, Martínez-Martínez et al., 2002), as evidenced by the

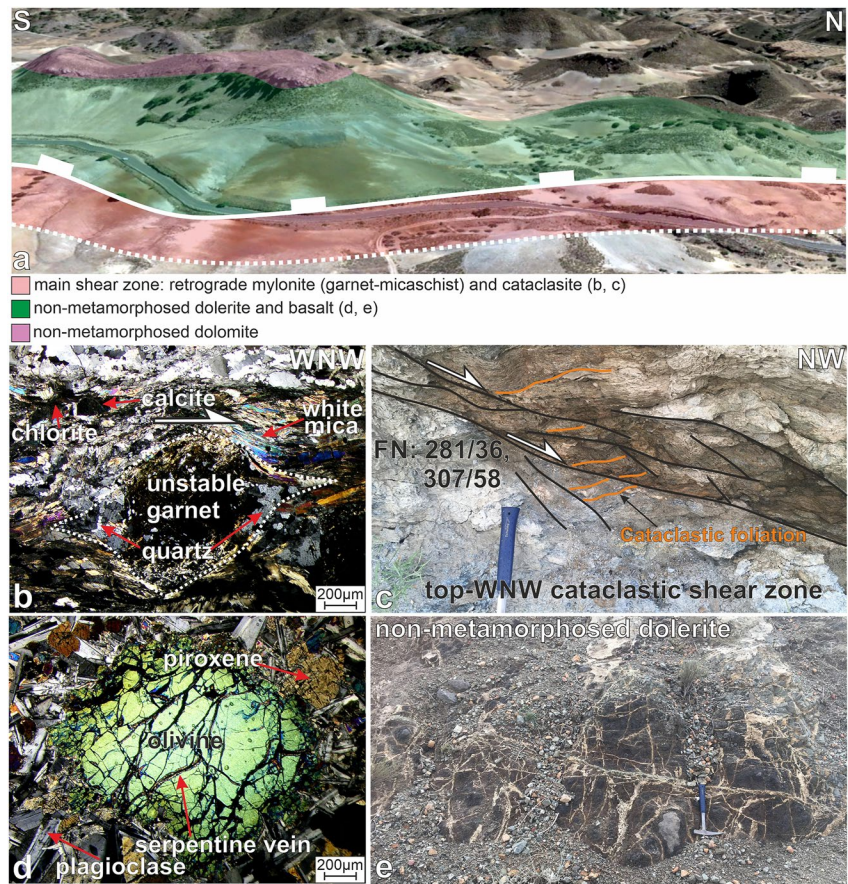


Figure 6. (a) Interpreted satellite image showing a typical exposure of the main extensional detachment (BMZ). The location of the exposure is given on Figure 1b (Key outcrop 7). (b) Cross-polarized thin section picture of the retrogressed garnet-micaschist directly underlying the BMZ. The asymmetry of the garnet + quartz + white mica clast suggests top-WNW sense of shear. (c) Retrograde mylonite reworked as a cataclasite within the main damage zone of the BMZ. Cataclastic shear bands and normal faults are dipping toward the WNW. (d) Cross-polarized thin section image of the non-metamorphic dolerite overlying the BMZ. The dolerite preserved its original igneous texture and composition. (e) Outcrop image of the non-metamorphic dolerite.

earlier described tectonic omission from the higher-grade footwall to the low-grade hanging-wall (see also Martínez-Martínez et al., 2002; Platt & Vissers, 1980).

Furthermore, the NFC in the footwall of the BMZ records strain localization during retrograde metamorphism (Agard et al., 2011), reflected in the development of retrograde shear fabrics across the dome and in the concentration of strain in the top part of the NFC. The metapelites in the core of the NFC preserve an early S_{0-1} foliation, overprinted by the dominant S_2 foliation (Figures 4a and 4e). Both foliations are overgrown by abundant and dominantly unoriented, retrograde chlorite (Figures 4a and 4e), implying that the core of the NFC was not affected by significant deformation during the growth of chlorite (for a detailed study also see Agard et al., 2011). In contrast, the top 100 m of the same metapelite formation directly underlying the top-WNW Marchal shear zone shows oriented chlorite (and albite) growth, defining the dominant stretching lineation and main foliation close to and within the shear zone (Figure 4b). Hence, the Marchal shear zone shows activity during retrograde metamorphism of the NFC, but this deformation did not propagate deeper into the Calar-Alto unit, producing a transition from oriented to unoriented chlorite growth from the flanks to the core of the dome. A similar trend is observed in the upper two tectonic units of the NFC (Ophiolite and Sabinas units). In the proximity of the Cuatro Amigos shear zone, the higher-temperature fabric of the garnet-micaschists is generally replaced by retrograde white mica, chlorite, and quartz (Figure 4d). Furthermore, the oriented growth of chlorite at the expense of the higher-temperature fabric is observed in the micaschists and metamafics of the Ophiolite unit, as well as in the orthogneiss of the Sabinas unit. The orthogneiss also exhibits bands of ultramytonites associated with top-WNW

sense of shear and growth of retrograde minerals such as sericite or chlorite (Figure 4g). Further away from the shear zone, garnets are typically better preserved (Figure 4c), retrograde stretching lineations are less frequent, and the dominant higher-grade sense of shear (top-NNW) is better preserved (Figure 1b). Hence, the Cuatro Amigos shear zone also shows activity during the retrograde metamorphism of the NFC, similarly to the Marchal shear zone.

4. White Mica Chemistry

The chemistry of the white micas dated by $^{40}\text{Ar}/^{39}\text{Ar}$ method (Section 5) was constrained by microprobe measurements, which allowed to characterize their Si versus Mg + Fe content (Figure 7c, the entire microprobe dataset is available in the Table S3). Variable Si content is generally interpreted as a result of the pressure-dependent

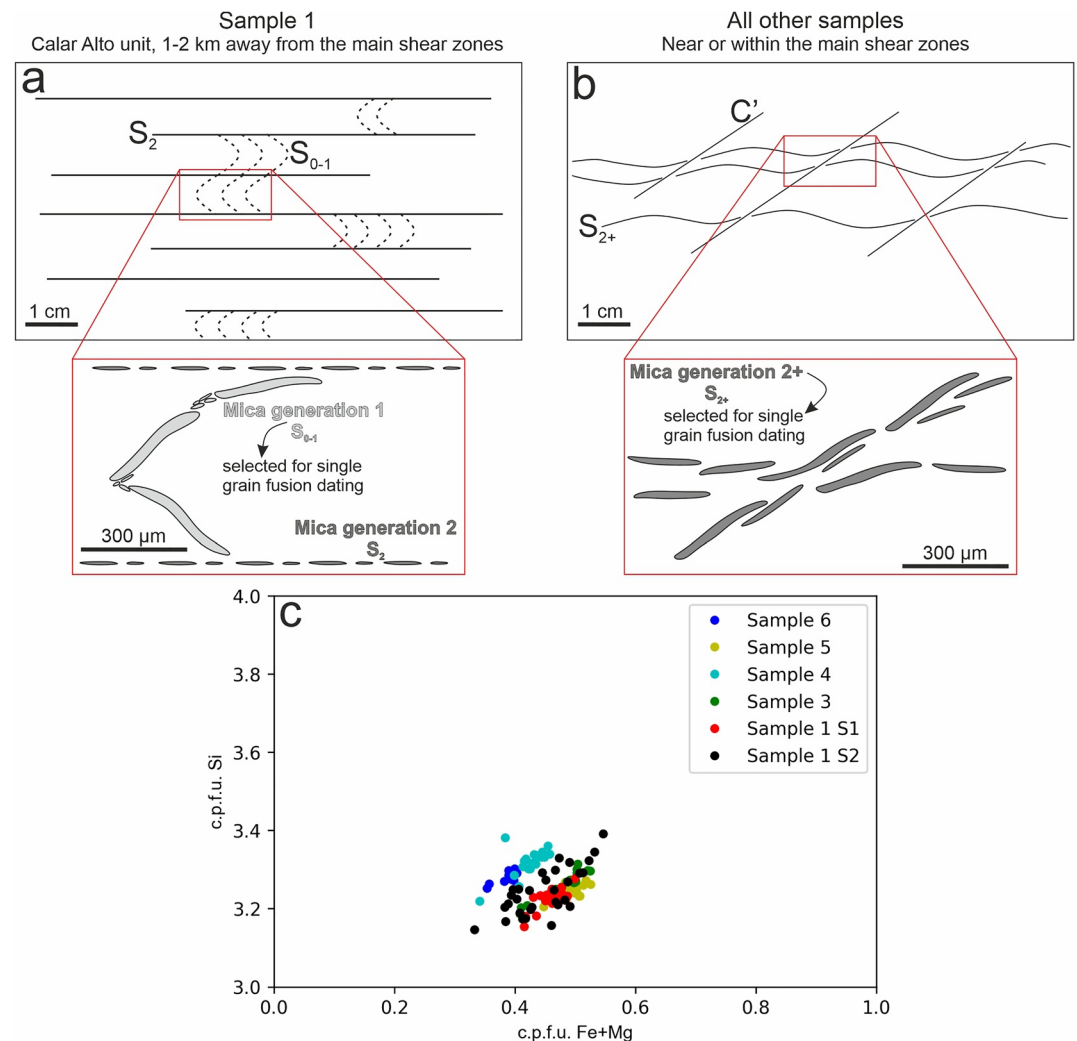


Figure 7. Relationship between metamorphic fabrics and different mica generations based on macroscopic and microscopic (see Figure 4) observations, together with the chemistry of mica populations dated by $^{40}\text{Ar}/^{39}\text{Ar}$. (a) Schematic 2D representation of the metamorphic fabrics and related mica generations in the relatively deep sections of the Calar-Alto unit (sample 1). Here the early S_{0-1} foliation is preserved, often defined by relatively large ($>250\ \mu\text{m}$) white mica grains, while the younger tectonic foliation is constituted by substantially smaller white mica crystals. Consequently, the 250–500 μm grain-size selection for the dating favored the sampling of the S_{0-1} fabric. (b) Schematic 2D representation of the metamorphic fabrics and related mica generations near or within the main shear zones of the eastern Sierra de Los Filábres (samples 2–6). Here the early S_{0-1} foliation is not preserved, hence all dated mica grains belong to the younger foliation(s), which developed during shear zone activity. (c) Si versus Fe + Mg c.p.f.u. (cations per formula unit) plot showing that all samples are characterized by a dispersion of Si content between ~ 3.2 and ~ 3.35 .

Tschermak substitution reaction, which represents a solid solution exchange reaction between muscovite and celadonite as end members, that is, $KAl_2[AlSi_3]O_{10}(OH)_2$ and $K[(Mg,Fe)Al][Si_4]O_{10}(OH)_2$, respectively. In common phengites, Si content is typically between 3.0 and 3.5 c.p.f.u. (cations per formula unit), where low-Si phengites are characteristic for low-pressure, while high-Si phengites are indicative of high-pressure (blueschist and eclogite facies) conditions (Massonne et al., 1995; Massonne & Schreyer, 1987). This pressure dependence of meta-pelite phengite composition in principle can be used as a first order guide for a distinction within each sample of different phengite generations.

We measured the composition of at least 10 mica grains in samples 1, 3, 4, 5, and 6. In sample 1, micas taken from the S_{0-1} and S_2 foliations (Figure 7a) were measured separately, while in other samples micas were selected from the dominant shear zone foliation (S_{2+}). Figure 7c shows that the Si content varies between 3.15 and 3.4 c.p.f.u., with every sample reaching maximum values of 3.3 or higher (Figure 7c). The dataset shows no major differences between the mean values of each sample, but shows different degree of dispersion: for example, sample six is much less dispersed than sample 3 (Figure 7c). In case of sample 1, micas derived from the S_{0-1} and S_2 foliations show no difference in the mean Si content, while the S_{2+} micas show a significantly larger dispersion (higher maximum and lower minimum values).

5. $^{40}Ar/^{39}Ar$ Dating

5.1. Sampling Strategy and Methodology

$^{40}Ar/^{39}Ar$ dating of white micas was performed with the objective to constrain the timing of metamorphic fabric formation and the activity of shear zones in our study area by selecting six samples from key areas of the eastern Sierra de Los Filábres (Figure 1b, see Figures 4d– and 4h for thin section images of dated samples). We selected one sample from the core of the NFC dome located 1–2 km away (vertically) from the main shear zones (Figures 4e and 7a), as well as five samples taken from different shear zones located along the flanks of the dome (e.g., 4f–4h and 7b). This strategy allowed exploring potential age differences between the S_{0-1} foliation, preserved only in the sample located in the core of the dome, and subsequent (S_2 and higher) shear zone foliations. We applied the $^{40}Ar/^{39}Ar$ dating of large ($\geq 250 \mu m$) white mica crystals with the multiple single grain fusion dating method (Uunk et al., 2018). The applicability of white mica $^{40}Ar/^{39}Ar$ single grain fusion dating approach for the detection of tectono-metamorphic events has been proven by numerous works (Lips et al., 1998; Lister & Forster, 2016; Porkoláb et al., 2019; Uunk et al., 2018; Wijbrans et al., 1990). The resetting of white mica Ar-systems may be achieved by thermal diffusion (allowing to constrain the timing of cooling below the closure temperature) or by deformation-induced or fluid-assisted (re)crystallization, which allows to constrain the timing of metamorphic fabric formation (e.g., Villa, 1998; Wijbrans & McDougall, 1986). Temperature-dependent resetting of white micas is a gradual process, and depends not only on the temperature itself but also on the duration of the overprinting event (Wijbrans & McDougall, 1986), as well as on the grain radius (de Jong et al., 1992). Hence, in case the metamorphic temperature was high enough and maintained long enough to reset all (small and large) mica crystals, homogenous age distribution of the dated single grains are expected (i.e., a single tectono-metamorphic event will be detected by the dated grains). In case one criteria was only partially sufficient, partial resetting may take place, producing heterogeneous age distribution, that is, detecting multiple resetting events and mixed ages in between (Lister & Forster, 2016; Uunk et al., 2018; Warren et al., 2012). Complete resetting of the white mica Ar-system by thermal diffusion is thought to require temperatures higher than typical values of greenschist-blueschist facies metamorphism ($>500^\circ C$, Harrison et al., 2009; Warren et al., 2012). If temperatures were not high enough (or the duration of heating not long enough) to reset the white mica Ar-system by thermal diffusion, some (or all) of the grains can still be reset by deformation-induced or fluid-assisted crystallization due to the formation of a tectonic foliation, producing similar homogenous or heterogeneous grain age distributions (Lister & Forster, 2016; Porkoláb et al., 2019; Villa, 1998).

White mica crystals of the crushed samples were separated from 250 to 500 μm sieve fractions using a Faul vibrating table and heavy liquid density-based separation. Carbonate and dust contamination were removed by HNO_3 treatment of the samples. Mica separated from six samples were selected for single grain fusion dating. The samples were packed in aluminum foil packages and stacked in an aluminum tube that was irradiated for 18 hr in the CLICIT facility of the Oregon State University TRIGA Reactor. For both irradiations the neutron flux was monitored by standard bracketing with the DRA sanidine standard with an age of 25.52 ± 0.08 Ma, modified from Wijbrans et al. (1995) to be consistent with Kuiper et al. (2008). Single grain fusion experiments

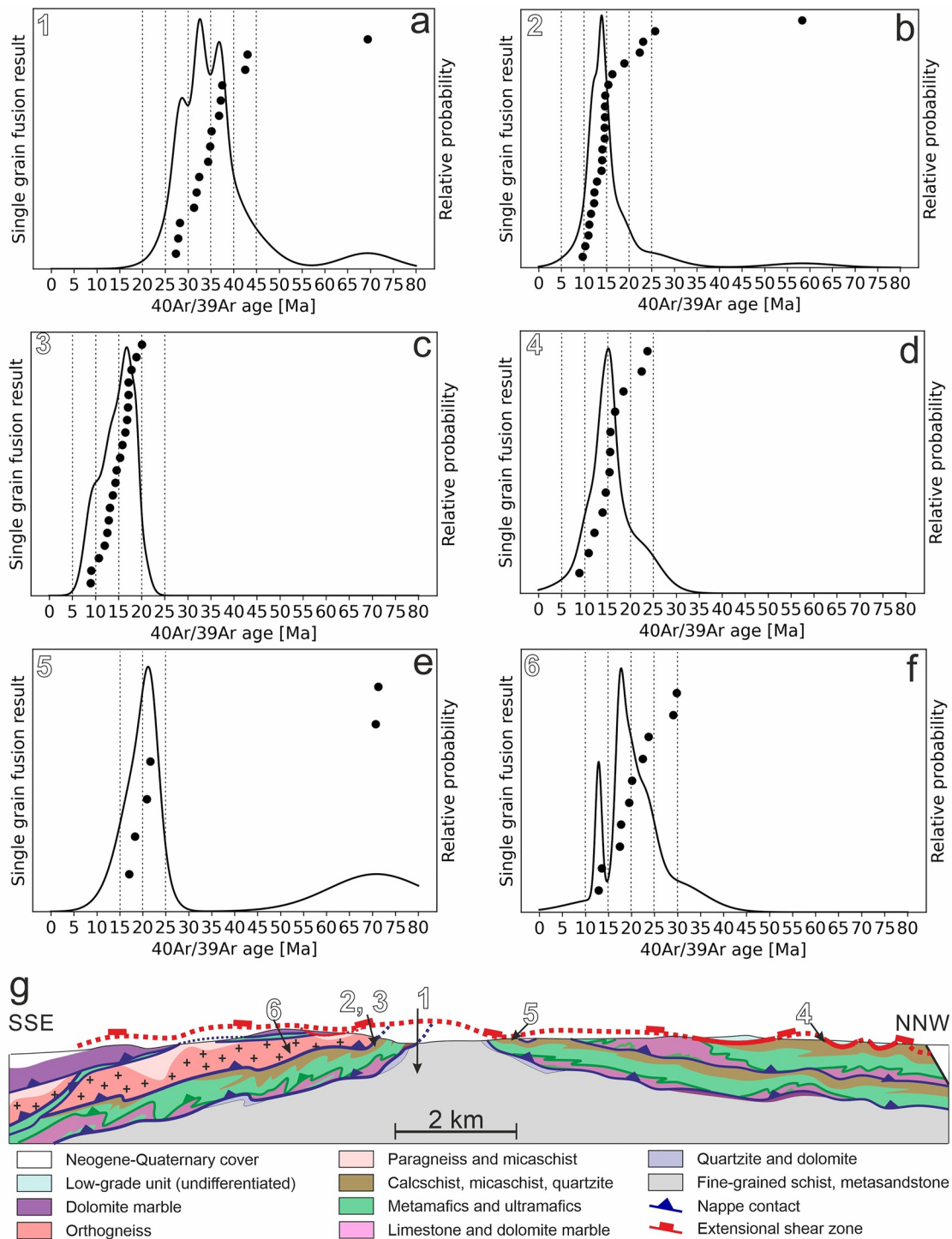


Figure 8. Results of single grain fusion white mica $^{40}\text{Ar}/^{39}\text{Ar}$ dating. (a–f) Plots of $^{40}\text{Ar}/^{39}\text{Ar}$ ages, where numbers indicate sample codes (for the map location of dated samples see Figure 1b). Black circles represent individual dated grains. Black lines show the relative probability, that is, the cumulated 1-sigma normal distributions of every grain age in the samples. Peaks in the black lines hence show most likely dates of resetting in the samples. (g) Cross-section through our study area showing the projected locations of the dated samples.

were carried out in the Vrije University Amsterdam argon geochronology laboratory with 25 W CO_2 laser heating samples loaded on Cu-trays (185 individual 2 mm diameter, 3 mm deep holes for single grains). The sample holder was connected to a three-stage extraction line and a quadrupole mass spectrometer (Schneider et al., 2009).

Data was reduced in ArArCalc 2.50 (Koppers, 2002). Procedure blanks were monitored and diluted air shots were measured in the sequence to track mass discrimination. Furthermore, we have constrained the chemistry of white micas in the samples dated with $^{40}\text{Ar}/^{39}\text{Ar}$ by microprobe measurements at Utrecht University, the Netherlands. Compositional analyses were acquired on an electron microprobe (JEOL JXA-8530F) for the following elements: Si, Al, Mg, Ca, Fe, Na, K, Mn, and Ti. For more details on the microprobe methodology we refer to the “method” sheet of Table S3 in Supporting Information S1.

5.2. $^{40}\text{Ar}/^{39}\text{Ar}$ Dating Results

The dated samples show a variety in age results as well as in the distribution of the single grain ages within individual samples. A group of three samples (samples 2, 3, and 4) display homogenous single grain age distributions with a relative probability peak at ~ 15 Ma (Figures 8b–8d). The grains that define the 15 Ma probability peak show ages between 12 and 22 Ma. Some grains with significant deviation from the mean are still present in these samples, showing older (20–25 Ma) or younger (10–12 Ma) ages. Sample 2 shows an outlier grain with substantially older (57 Ma) age. Sample 1 also shows a largely homogenous age distribution; however, the peak relative probability of the ages is significantly older, ~ 33 Ma (Figure 8a). The grains that define the probability peak are between 27 and 38 Ma, while two outlier grains are present in between 40 and 45 Ma, and one grain at 70 Ma. Sample 5 contains four grains close to 20 Ma, and further two at 70 Ma (Figure 8e), while sample 6 shows the most heterogeneous age distribution with three groups of grains at 12–14 Ma, 17–24 Ma, and 28–30 Ma (Figure 8f).

The location and microstructure of the dated samples highlight the possible importance of the age differences between Sample 1 and all the other samples (Figures 7a, 7b and 8g). Sample 1 was collected from the pelitic schist formation of the Calar-Alto unit, relatively far from the major shear zones in the area. This sample is the only one to preserve S_{0-1} foliation in crenulations (Figure 7a), and thus probably preserved earlier mica generation(s) compared to the other samples (Figure 7b). Furthermore, the grain size of the white micas in the relic S_{0-1} foliation (typically 100–300 μm) is substantially larger than the grain size of white micas in the pervasive S_2 foliation (typically 50–150 μm , Figures 4e and 7a). Hence, the dated micas belong to the older S_{0-1} foliation, as all the selected single grains were larger than 250 μm (Figure 7a). The mean age of 33 Ma of this sample is significantly older than the mean age of the other samples (15–20 Ma) which were collected near (sample 6) or from the major shear zones (samples 2, 3, 4, 5, Figure 8g). In these samples the oldest S_{0-1} foliation is completely obliterated by the superposed foliation and shear fabric development due to shear zone activity, resulting in the formation of S_2 or younger shear zone foliations (Figure 7b). Samples 2, 3, and 5 were collected from micaschists of the Ophiolite unit, incorporated into the shear zone that emplaced the Carboniferous formations of the Sabinas unit on top of the Ophiolite unit. The shear zone was later likely reactivated (or progressively used) during the exhumation of the NFC (see Section 3.2.3). Sample 4 was collected from the retrograde garnet-micaschists incorporated in the BMZ that separates high-grade and low-grade units, while sample 6 was collected from a mylonitic horizon of the Carboniferous orthogneiss of the Sabinas unit.

6. Discussion

6.1. Interpretation of $^{40}\text{Ar}/^{39}\text{Ar}$ Ages and Timing of Tectono-Metamorphic Events

Numerous studies have shown that Ar-loss in white micas is a complicated process, where thermal diffusion might only play a limited role in the resetting of the Ar-system, particularly when significant deformation or fluid flow is present in the given rock volume (Harrison et al., 2009; Lister & Forster, 2016; Uunk et al., 2018; Villa, 1998; Warren et al., 2012). Our results are in agreement with in-situ laser $^{40}\text{Ar}/^{39}\text{Ar}$ white mica ages reported by Augier, Agard, et al. (2005), which shows older ~ 45 –25 Ma ages for the preserved S_{0-1} foliation when compared with the ~ 22 –12 Ma ages in places where such foliation was overprinted by the fabric of a shear zone. Our results and those of Augier, Agard, et al. (2005) indicate that structural criteria (preservation of a tectonic foliation) correlate with the age results, which implies that temperature is not the dominant mechanism of resetting. We hence argue that the dominant resetting mechanism in our samples was deformation- and possibly fluid-induced (re)crystallization during the development of tectonic foliations. Along these lines white micas constituting an older foliation (S_{0-1}) in the metapelites of the Calar-Alto unit yield older age clusters compared to samples where micas constitute younger fabrics (S_2 or younger foliations developed during shear zone activity).

Furthermore, these samples are located at a vertical distance of ca. 1–2 km below the main shear zones (Marchal shear zone, see Figures 1c and 1d in Augier, Agard, et al. (2005)) and do not exhibit evidence for significant deformation during the activity of these overlying shear zones (22–12 Ma). Hence, we assume a very limited deformation- or fluid flow-induced Ar-loss in these samples during the activity of the main shear zones. It follows that peak temperatures (ca. 470–550°C) in the Calar-Alto unit (Augier, Agard, et al., 2005; Li & Massonne, 2018; Santamaría-López et al., 2019) were not high enough (or not sustained long enough) to facilitate efficient thermal diffusion in the metapelites.

Several studies have suggested that excess argon might be responsible for the presence of older than early Miocene white mica $^{40}\text{Ar}/^{39}\text{Ar}$ ages in the NFC (Behr & Platt, 2012; de Jong, 2003; De Jong et al., 2001; Kirchner et al., 2016; Platt et al., 2006). Excess argon incorporation in white micas has been attributed to sub-microscopic illitization during late-stage hydraulic fracturing, where the density of the fracture network controls the grade of illitization and hence the amount of excess argon incorporation on the scale of individual grains (De Jong et al., 2001). This process resulted in highly varying $^{40}\text{Ar}/^{39}\text{Ar}$ ages in samples of the Carboniferous orthogneiss, somewhat similar to sample 6 in our study selected from the same rocks (Sabinas unit, Figures 2 and 7). In this sense, significant age variations in sample 6, and possibly the significantly older, outlier grains in the other samples could also be explained by excess argon incorporation, not only by partial resetting (inherited argon). However, sample 1 shows a consistent, homogenous distribution of older ages between 27 and 38 Ma, which do not exhibit the typical variance caused by excess argon. In addition, the effect of excess argon (if present) is expected to be more profound in the coarser grained rocks such as the micaschists of the Ophiolite unit (samples 2, 3, 4, 5, yielding 12–22 Ma grains) compared to the fine grained schists of the Calar-Alto unit (sample 1, yielding 27–38 Ma grains), therefore predicting that sample 1 should be less affected by this process (De Jong et al., 2001). Consequently, the above described correlation of the observed structural criteria (preservation of an older foliation far from the shear zones) with the older age clusters demonstrated in Augier, Agard, et al. (2005) and in this study is a more logical explanation for the variety of age data than assuming an unclear presence of excess argon in those samples. All these arguments considered, we interpret our white mica $^{40}\text{Ar}/^{39}\text{Ar}$ ages as a record of two different fabric forming periods, that is, (re)crystallization of white micas as a result of deformation events: (a) a Paleogene fabric evolution recorded by Sample 1 in the Calar-Alto unit (38–27 Ma), and (b) an early-middle Miocene fabric evolution recorded by the samples within or in the proximity of the main shear zones (22–12 Ma). Outlier grains (four grains in all samples) with significantly older age results (60–70 Ma) and the significant age variation (heterogenous distribution) in sample 6 are possibly the result of inherited or excess argon in the samples.

Accounting for the full range of existing geochronological ages (Figure 9) shows that our Paleogene white mica $^{40}\text{Ar}/^{39}\text{Ar}$ ages and those of Augier, Agard, et al. (2005) are in agreement with amphibole $^{40}\text{Ar}/^{39}\text{Ar}$ and monazite U-Th-Pb data (Li & Massonne, 2018; Monié et al., 1991). Miocene U-Pb zircon, Lu-Hf garnet, and $^{87}\text{Rb}/^{86}\text{Sr}$ multimineral ages that are supplemented by thermodynamic data constraining the P-T conditions of the dated minerals outline a second episode of prograde, HP-LT metamorphism (Kirchner et al., 2016; Platt et al., 2006; Sánchez-Vizcaíno et al., 2001). Accepting both sets of ages and their interpretations as burial-related metamorphism, one could argue that the NFC might have experienced a long-lasting, multi-episode (at least two) burial process, starting in the Paleogene and finishing during the early Miocene (see Section 6.4 for discussion on the possible geodynamic scenarios).

6.2. Superposition of Miocene Thrusting and Extension: The Mechanics of Exhumation and the Structural Definition of the NFC and the AC

Our kinematic data suggest that the main nappe contacts of the eastern Sierra de Los Filábres formed during moderate-temperature shearing after peak metamorphic conditions, with a kinematics of top to NW-NNW in present-day orientation. Furthermore, these shear zones display significant evidences of activity during the retrogression (marked by oriented chlorite growth) and exhumation that took place with a general top to WNW-WSW kinematics (in present-day coordinates). The transition from higher to lower metamorphic temperatures during the activity of these shear zones appears to be accompanied also by a change in the pressure-dependent Si content of the phengites of the shear zone foliations, ranging from 3.2 to 3.4 c.p.f.u (Samples 3, 4, 5, 6 on Figure 7c). The kinematic observations imply that the shear zones progressively rotated from top to NW-NNW shearing possibly during burial and early exhumation to top to WNW-WSW shearing during the subsequent exhumation

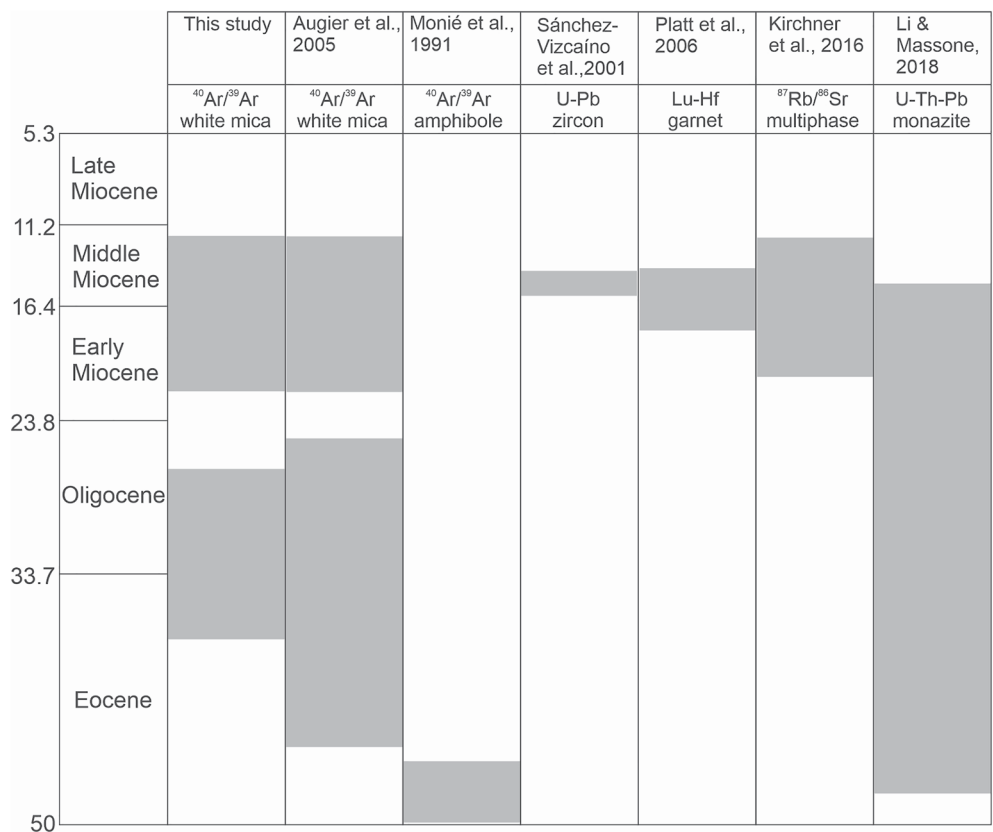


Figure 9. Summary of published geochronological results constraining the timing of tectono-metamorphic events in the NFC.

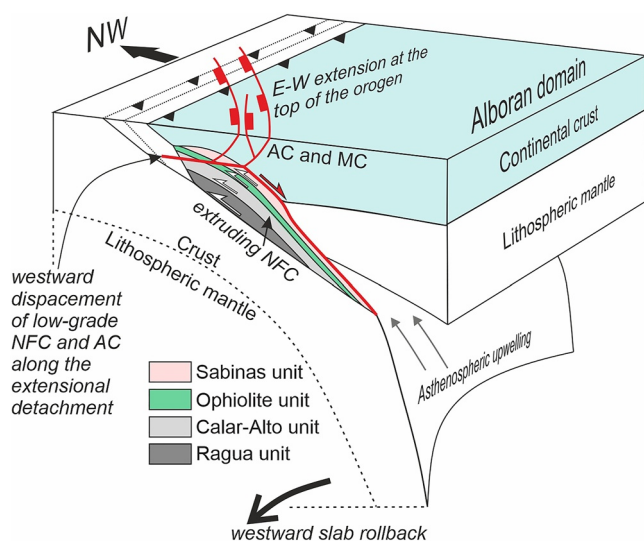


Figure 10. Schematic 3D sketch of the early exhumation (extrusion) stage of the NFC in the early-middle Miocene showing the superposition of nappe stacking and extensional detachment (BMZ) formation. Note that the original, ~top-NW nappe contacts were obliquely cut by the ~top-W BMZ that localized at the brittle-ductile transition zone. Therefore, it is possible that low-grade and high-grade metamorphic equivalents of the same formations from the same nappe units are juxtaposed by the BMZ.

to mid-crustal levels. This significant change in the sense of shear during exhumation implies a different strain and stress pattern for mid-crustal levels compared to the subduction zone, most likely related to the localization of the main, top-WNW-WSW extensional detachment system (BMZ) at the brittle-ductile transition zone (BDTZ, Martínez-Martínez et al., 2002). Our results hence indicate that the exhuming NFC nappes were captured by the BMZ when reaching the BDTZ, which facilitated their further (final) exhumation and resulted in oblique shearing with respect to the nappe stacking direction (Figure 10). This interpretation is consistent with existing extrusion models of the NFC, where the formation of the BMZ at the brittle-ductile transition zone took place coevally with the contractional exhumation (i.e., extrusion) of the NFC (Behr & Platt, 2012; Booth-Rea et al., 2005, 2015). These interpretations are further supported by the observation of E-W trending upright folding, related to N-S contraction, interpreted to be coeval to and also younger than the formation of the BMZ (Augier, Agard, et al., 2005; Martínez-Martínez et al., 2002). Therefore, in agreement with these studies, we interpret the exhumation of the NFC to be the result of an interplay between the extrusion of subducted crust in the deeper segments of the subduction zone, and coeval upper crustal extension in the orogen (Figure 10).

Established models of extrusion have shown that nappe formation and exhumation of deeply subducted continental material creates uplift and associated extension in the orogenic upper crust (Chemenda et al., 1996, 1997; Hacker et al., 2000; Herwegh et al., 2017; Platt, 1986). Applying these models to the Betics implies that the initial buoyancy-driven extrusion of

the subducted NFC may have triggered uplift and hence the localization of the BMZ, which in turn accommodated the extrusion of the subducted crust. The extrusion of the NFC and the localization of the BMZ was facilitated by the westward migration of the slab, that created space for rock exhumation as well as for asthenospheric upwelling, which resulted in the observed high-T overprint (reheating) of the NFC during exhumation (Booth-Rea et al., 2005, 2015; Santamaría-López et al., 2019). The highly oblique (almost orthogonal) kinematics of the top-W or SW BMZ compared to the original, top-NW nappe stacking direction observed in Sierra de Los Filábres (Figure 10, Behr & Platt, 2012; Martínez-Martínez et al., 2002; Platt, Allerton, et al., 2003) is more compatible with an orogen-parallel (or trench parallel) extension mode that creates elongation domes associated with orogen perpendicular shortening during orogenic building (e.g., Brun, 1983; Rey et al., 2011), as previously suggested for the NFC (e.g., Behr & Platt, 2012; Jolivet et al., 2021; Martínez-Martínez et al., 2002), or observed elsewhere, such as in case of the Tauern or Danubian windows of the Eastern Alps and South Carpathians (e.g., Matenco & Schmid, 1999; Scharf et al., 2013).

The NFC and AC are not only defined as tectonic units, but also as paleogeographic units juxtaposed by thrusting in a subduction zone. Their use in paleogeographic interpretations must be based on the modern nappe structure (i.e., different units bounded by thrusts). However, the current definition of the AC and the NFC within our study area is also based on the contrast in metamorphic grade created by the tectonic omission along the BMZ, instead of the original thrusts (Martínez-Martínez et al., 2002). Using a detachment between the AC and NFC as a nappe definition would be valid if the extensional detachment reactivated exactly the original nappe contacts, with an opposite sense of shear. This way of reactivating nappe contacts has been interpreted elsewhere in the Mediterranean to be an important mechanism of exhumation of metamorphic rocks (e.g., Jolivet et al., 2010). However, in case of the Betics, the highly oblique kinematics of the superposed nappe stacking and extension implies that the BMZ obliquely cut through the nappe-stack (Figure 10), creating a tectonic omission between the NFC and the AC, and possibly reactivating pre-existing shear zones during the late-stage formation of the extensional dome (see also Martínez-Martínez et al., 2002).

Due to the oblique displacement along the BMZ with respect to the original nappe stacking shear zones, low-grade metamorphic formations that originally belong to the NFC are also expected to be observed in the hangingwall of the BMZ, overlying their high-grade stratigraphic equivalents in the footwall (Figure 10). Examples for such formations could be the low-grade or non-metamorphosed basalts, dolerites, and gabbros (Figure 6), which are the protoliths of the high-grade amphibolites or eclogites in the Ophiolite Unit across the BMZ. Similarly, the low-grade lithologies commonly assigned to the AC along the northern flank of the eastern Sierra de Los Filábres such as Paleozoic phyllites and Triassic dolomites have high-grade equivalents below the BMZ (schists and dolomite marbles). Therefore, we suggest that due to the oblique superposition of nappe stacking and extension, the low-grade formations in our study area are not necessarily part of the AC, but may also be part of the NFC in terms of paleogeographic provenance, while also justifying the existence of high-grade AC metamorphic rocks outside our study area. Ultimately, we conclude that a separation between the BMZ creating the observed tectonic omission and the nappe stacking reflecting the paleogeographic provenance of continental units should be further pursued in the Sierra de Los Filábres and elsewhere in the internal Betics.

6.3. Origin and Emplacement of the (Ultra)mafic Unit

The mafic-ultramafic rock succession of the NFC is most commonly interpreted in the context of a magma-poor, hyper-extended (Iberian-derived) continental margin, which contains intruded mafic dykes as well as areas with mantle rocks exhumed to the seafloor (e.g., Booth-Rea et al., 2015; Gomez-Pugnaire & Munoz, 1991; Laborda-López et al., 2020). The same rock succession is also interpreted as a separate tectonic unit (Ophiolite unit, Puga et al., 2002, 2011), representing the metamorphosed remnants of an independent ophiolite sheet. Our observations are consistent with large parts of both interpretations, which in our view are not exclusive.

A key observation is the presence of a mixture of sedimentary and (ultra)mafic rocks in an original protolith, interpreted as an ophiolitic mélange. The observation of the S_{2-3} foliations in serpentinites (serpentine schists) that is coherent with those of the neighboring metasedimentary rocks indicates that the mélange formation predates the D_2 tectono-metamorphic event. The combination of an olistostrome and a shear zone is typical for an ophiolitic mélange, which forms by gravity emplaced (ultra)mafic blocks and rocks scraped from the underlying continental formations. The different blocks are buried in a sedimentary matrix derived partly from alteration reactions of (ultra)mafic minerals, and are thrust by ophiolite sheets during their obduction over continental

margins (Figure 11c). Such ophiolitic mélanges have been described from ophiolite complexes worldwide, such as the ones observed in the Dinarides or Hellenides (Andersen et al., 1990; Schmid et al., 2008; Yilmaz & Maxwell, 1984). The mélange of the (ultra)mafic unit cannot simply represent a brittle shear zone where the different lithologies are mixed in the damage zone, because the sedimentary olistostrome fabric of the original protolith is still preserved in some outcrops (e.g., Figures 5d and 5e), although significantly affected by the subsequent shearing during burial and furthermore crosscut by late extensional shear zones and normal faults during exhumation.

The interpretation of an ophiolitic mélange associated with the obduction of ophiolites does not exclude the presence of a hyper-extended continental margin, whose continental mantle could have been connected to—a probably narrow or embryonic—oceanic lithosphere (Figure 10b). Therefore, there is no conflict between ophiolite and hyper-extended continental margin interpretations, as both can be part of the same paleogeographic domain.

6.4. Possible Geodynamic Scenarios

The geodynamic evolutionary model of the NFC critically depends on the interpretation of geochronological data. The current scientific understanding of isotopic closure during a multiphase tectono-metamorphic evolution is incomplete; hence, geochronological data do not offer a direct single solution yet. As a consequence of this uncertainty, arguments have been put forward for the invalidation of either Paleogene or Miocene HP-LT fabric age data. For example, Behr and Platt (2012) or Kirchner et al. (2016) argues that Paleogene Ar/Ar ages are unreliable due to excess argon in white micas, while Bessi ere et al. (2022) argues that successful dating of burial requires exceptionally preserved HP-LT fabrics based on samples from the AC. In our view, arguments for and against the validity of the two age groups are not conclusive yet, which warrants the consideration of different timing scenarios for the subduction of the NFC, depending on the interpretation of the age data. A further variable in the geodynamic solutions is the origin of the Ophiolite unit. Our observations of the ophiolitic mélange suggest that subduction of the NFC below the AC and MC may have been preceded by the obduction of the Ophiolite unit. In this case, the burial evolution of the continental NFC must contain two main phases. Three possible geodynamic scenarios in this overall context are given below.

6.4.1. Eocene Subduction-Slow Exhumation

If Paleogene geochronological ages (Figure 9) are accounted for to reflect tectonic burial and metamorphism, there are two possible solutions. The first solution considers Paleogene burial followed by slow exhumation during the Miocene, hence relating Miocene ages to exhumation (Augier, Agard, et al., 2005; Bessi ere, 2019; Bessi ere et al., 2022; Li & Massonne, 2018; Moni e et al., 1991). This interpretation correlates the NFC with the same paleogeographic continental unit as the AC and MC or the Upper Sebtides in the Moroccan Rif belt (AlKaPeCa unit, Bouillin et al., 1986), which record similar Paleogene ages of metamorphism (Bessi ere et al., 2022; Marrone, Moni e, Rossetti, Aldega et al., 2021; Marrone, Moni e, Rossetti, Lucci et al., 2021; Moni e et al., 1994; Platt et al., 2005). This solution is consistent with currently available kinematic and P-T data; however, it is difficult to reconcile with the very limited (<100 km) convergence in the Eocene, considering that all three of the AC, Ophiolite unit, and continental NFC must be stacked and subducted below the MC. This solution also requires the assumption that Miocene ages of HP-LT fabrics in the NFC (Kirchner et al., 2016; Platt et al., 2006; S anchez-Vizca ino et al., 2001) belong to insufficiently preserved HP-LT mineral assemblages.

6.4.2. Gradual Eocene-Early Miocene Burial and Fast Exhumation

The second solution is a long-lasting, gradual burial of the NFC, starting in the Paleogene and terminating during the early Miocene, followed by fast exhumation. This solution can account for the full range of published geochronological data of HP-LT fabrics (not discarding any published data as unreliable), which points toward both Paleogene (Augier, Agard, et al., 2005; Li & Massonne, 2018; Moni e et al., 1991) and Miocene (Kirchner et al., 2016; Platt et al., 2006; S anchez-Vizca ino et al., 2001) episodes of HP-LT metamorphism; an idea that has already been proposed by Li and Massonne (2018) based on monazite dating. Multiple HP-LT episodes during a gradual burial history is also consistent with our mica chemistry data, which shows that both the S_{0-1} (Paleogene) and S_{2+} (Miocene) foliations contain high-Si phengites, generally characteristic for HP metamorphism (Figure 7c). In this scenario, the Paleogene burial can be related to the obduction of an oceanic lithosphere connected with a hyper-extended continental margin over the continental NFC. The obduction of oceanic lithosphere or arc-continent collisions are commonly associated with regional burial metamorphism of continental

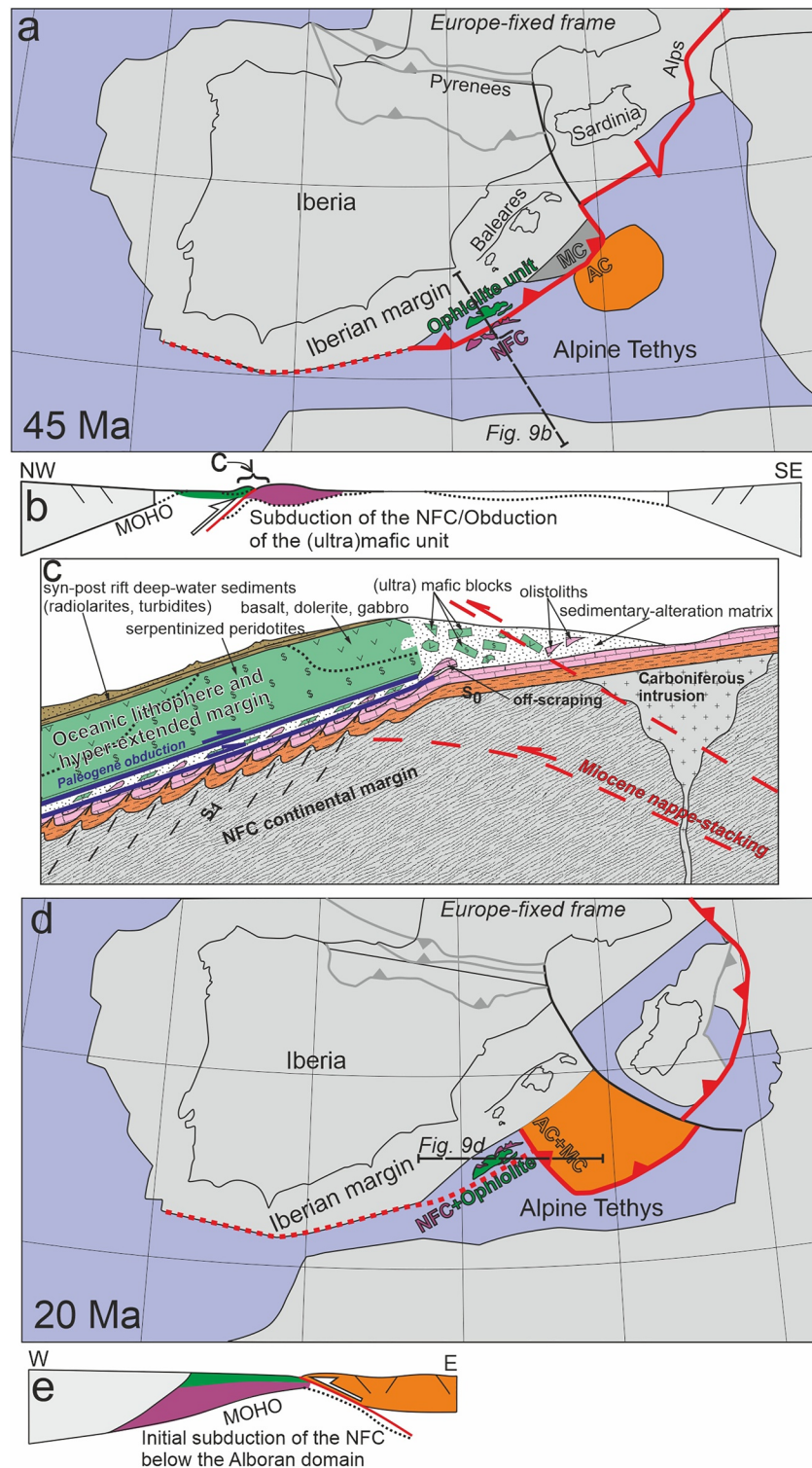


Figure 11. Tectonic reconstruction of the Western Mediterranean region highlighting the relevant tectonic units of the Betics, modified after van Hinsbergen et al. (2020) in order to visualize the hypothesis of long-lasting, gradual burial of the NFC. (a) Snapshot at 45 Ma showing the Paleogene subduction of the NFC and the AC below dominantly oceanic (Ophiolite unit) and continental (MC) upper plate segments, respectively. (b) Schematic cross-section through the 45 Ma reconstruction snapshot. (c) Schematic sketch of the proposed obduction of the hyper-extended margin connected to a piece of oceanic lithosphere, magnified from the cross-section of (b), highlighting the possible positions of different lithologies (mafic and ultramafic rocks capped by syn-post-rift sediments, ophiolitic mélange, and the downgoing continental formations), observed in the continental NFC and Ophiolite unit. (d) Snapshot at 20 Ma showing the initial early Miocene subduction of the NFC below the Alboran domain containing the MC and the AC. (e) Schematic cross-section through the 20 Ma reconstruction snapshot.

margins (e.g., Agard & Vitale-Brovarone, 2013; Goffé et al., 1988; Porkoláb et al., 2021; Pourteau et al., 2013; van Hinsbergen et al., 2016). In this scenario, the Paleogene white mica $^{40}\text{Ar}/^{39}\text{Ar}$ ages of the relic S_{0-1} foliation in the continental Calar-Alto unit can be explained by burial metamorphism during the obduction of the Ophiolite unit (Figure 11c), whose record is preserved only in the deeper sections of the Calar-Alto unit, at far distances from the Miocene shear zones (Figures 7a and 8g). A detailed explanation and related paleogeographic reconstruction for this scenario is presented in Section 6.5. We emphasize that more petrological work is needed for validating or invalidating this model (similarly to the other scenarios); in particular, by clearly demonstrating long-lasting or multi-episode HP-LT fabric growth. We also note that mica chemistry (Figure 7c) alone is not sufficient to prove the existence of multiple HP-LT fabrics, as the Si-content—while being pressure-sensitive—also depends on the chemical composition and the temperature (Massonne & Schreyer, 1987).

6.4.3. Early Miocene Subduction and Fast Exhumation

In the third scenario, where Paleogene geochronological ages are not interpreted as burial metamorphism, the Miocene subduction of the entire (continental and oceanic) NFC remains the simplest solution (Booth-Rea et al., 2015; Kirchner et al., 2016; Platt et al., 2006; Sánchez-Vizcaíno et al., 2001). Given the currently incomplete understanding of isotopic closure and the related overall debate on the reliability of different geochronological data, we do not exclude this interpretation. However, the presence of a metamorphosed ophiolitic mélange stacked in the NFC units and the structural dependence of Ar/Ar ages are not straightforward to reconcile with this interpretation.

6.5. Tectonic Reconstruction for the Gradual Paleogene—Early Miocene Burial Hypothesis

Reconstructions of the Betics orogen have placed the continental NFC either in the AlKaPeCa terrane (i.e., a pre-subduction microcontinent or extensional allochthon), to explain Paleogene burial ages (solution of Section 6.4.1, e.g., Bessière et al., 2021; Vissers et al., 1995), or on the SE-Iberian margin, to explain Miocene burial ages (solution of Section 6.4.3, e.g., Moragues et al., 2021; Platt et al., 2006). Based on the combination of our results and literature data (e.g., Figure 9), we suggest that these interpretations are not mutually exclusive, and we envisage a model of long-lasting burial for the NFC that explains both Paleogene and Miocene ages of prograde metamorphism.

The Paleogene burial ages of the continental NFC place these units within the AlKaPeCa terrane, which differs from recent paleogeographic reconstructions (e.g., van Hinsbergen et al., 2020; van Hinsbergen et al., 2014). The burial of the NFC and AC are simultaneous, and given the very low convergence rates of only mm/year in the Eocene, this requires that the NFC and AC were lateral paleogeographic units that were both part of the AlKaPeCa terrane (part of the same continental block or laterally separated blocks, Figure 11a). The AC was buried below the MC that was presumably either the most distal forearc of Iberia, or a continental nappe system that was also derived from AlKaPeCa. There is no structurally higher unit above the MC to give a conclusive answer. The NFC was buried below oceanic crust (the Ophiolite unit), and we therefore envisage that the subduction zone transitioned from along the Iberian continental margin into the oceanic crust of the Alpine Tethys, such that a narrow strip of oceanic crust was located in the upper plate, below which the NFC subducted in Eocene times (Figures 11a–11c).

The Miocene burial of the NFC plus the overlying ophiolites below the AC requires that the pivot point around which the trench rotated was located between the two units (Figure 11d). As a result, the NFC and the overlying Ophiolite unit were part of the Iberian margin (lower plate), whilst the AC was part of the upper plate, that is, the Alboran domain (Figures 11d and 11e). The Alboran domain started to thrust over the composite NFC–Ophiolite unit in the Early Miocene, with an almost opposite vergence compared to Paleogene thrusting (Figures 11a and 11d). Peak metamorphic conditions in the (ultra)mafic rocks were achieved during this Miocene stage. This Miocene history is almost the same as in van Hinsbergen et al. (2020). The difference is that instead of assuming an undeformed Iberian margin, our reconstruction implies that the Iberian margin already hosted an Eocene fold-thrust belt related to ophiolite obduction, prior to the Early Miocene subduction below the Alboran domain.

This model accounts for all previously interpreted Paleogene and Miocene episodes of prograde metamorphism (subduction) in the continental formations of the NFC, corresponding to Paleogene and Miocene geochronological data, and only one, Paleogene phase of subduction in the AC, while keeping the consistency with all other geological and geophysical data described in van Hinsbergen et al. (2020). It also explains the presence of an

ophiolitic mélangé associated with the (meta-)mafic and ultramafics of the Ophiolite Unit by incorporating a Paleogene obduction (Figure 11c). The Paleogene obduction might also play an important role in the rheological weakening of the Iberian margin, which might be important for facilitating the westward rollback of the slab along the margin (Chertova et al., 2014). In our reconstruction, the NFC undergoes $\sim 25^\circ$ clockwise rotation following the early Miocene subduction. As the initial Miocene burial direction was top-W (Figure 11d), the presently observed NW-SE orientation of the moderate-temperature stretching lineations are explained by the clockwise rotation (the originally E-W trending lineations are rotated to NW-SE). Furthermore, this rotation might also explain the observed top-SSW vergence in and above the ophiolitic mélangé formation (Figures 5a and 5c): the Paleogene vergence of obduction was top-SE (Figure 11a), which rotates to a more southerly (\sim top S) direction after the early Miocene.

7. Conclusions

We presented the results of a structural analysis and single grain fusion $^{40}\text{Ar}/^{39}\text{Ar}$ dating of white micas to address the tectonic and paleogeographic evolution of the Betics mountain range in SE Spain. We refined the tectonic subdivision of the eastern Sierra de Los Filábres to document strain localization during the burial and exhumation of the NFC. Our results show that the main nappe contacts in the NFC were active during the Miocene continental subduction-exhumation cycle both at moderate-temperature metamorphic conditions following burial and at retrograde conditions during the late exhumation stage of the NFC. The kinematics of shearing along the nappe contacts gradually changed from top-NNW to top-W as the rocks were being exhumed and captured by the top-W-WSW extensional detachment (BMZ) localized at the brittle-ductile transition zone. The observed change in the sense of shear during exhumation suggest that the BMZ obliquely cut the inherited nappe contacts, hence the low-grade formations exposed along the northern flank of the Sierra de Los Filábres do not necessarily belong to the AC, but may also belong to the NFC in terms of paleogeographic provenance. We documented the existence of an ophiolitic mélangé formation, which suggests that the (ultra)mafic succession of the NFC (Ophiolite unit) is a dismembered ophiolite sheet originally emplaced by an obduction process. White mica $^{40}\text{Ar}/^{39}\text{Ar}$ ages correlate with the preservation or obliteration of an early, relic, metamorphic fabric in the rocks of the NFC. Our white mica $^{40}\text{Ar}/^{39}\text{Ar}$ ages hence largely record Ar-loss due to deformation/fluid-induced recrystallization during two fabric-forming periods at 38–27 Ma and 22–12 Ma. The combination of our results with previously published geochronological and petrological data in the NFC allows for three different geodynamic solutions due to the currently limited understanding of isotopic closure during a multiphase tectono-metamorphic evolution. These are (a) Eocene burial and slow exhumation; (b) our newly proposed hypothesis, Eocene-Early Miocene gradual burial and fast exhumation; and (c) Early Miocene burial and fast exhumation. The newly proposed hypothesis of Eocene-Early Miocene gradual burial (subduction) accounts for Paleogene obduction of the Ophiolite unit over the continental formations of the NFC, which explains Paleogene geochronological data in the continental NFC as well as the presence of an obduction mélangé in the Ophiolite unit.

Data Availability Statement

Structural data for this research (data of stretching lineations with associated shear sense directions and fold axes) are available in Table S1 in Supporting Information S1. The description and coordinates of the dated samples are available from Table S2 in Supporting Information S1. The microprobe data of dated white mica populations are available from Table S3 in Supporting Information S1. The supporting tables are available from the Zenodo data repository platform (<https://doi.org/10.5281/zenodo.5707184>).

Acknowledgments

The research presented in this paper was funded by the European Union's MSCA-ITN-ETN Project SUBITOP 674899. Hans de Bresser and Frits Hilgen are gratefully acknowledged for their field introduction to the geological world of the Betics. Guillermo Booth-Rea, Patrick Monié, and Romain Augier are gratefully acknowledged for their constructive suggestions that have greatly improved the original manuscript.

References

- Agard, P., Augier, R., & Monié, P. (2011). Shear band formation and strain localization on a regional scale: Evidence from anisotropic rocks below a major detachment (Betic Cordilleras, Spain). *Journal of Structural Geology*, 33(2), 114–131. <https://doi.org/10.1016/j.jsg.2010.11.011>
- Agard, P., & Vitale-Brovarone, A. (2013). Thermal regime of continental subduction: The record from exhumed HP–LT terranes (New Caledonia, Oman, Corsica). *Tectonophysics*, 601, 206–215. <https://doi.org/10.1016/j.tecto.2013.05.011>
- Andersen, T. B., Skjerlie, K. P., & Furnes, H. (1990). The Sunnfjord Melange, evidence of Silurian ophiolite accretion in the west Norwegian Caledonides. *Journal of the Geological Society*, 147(1), 59–68. <https://doi.org/10.1144/gsjgs.147.1.0059>
- Augier, R., Agard, P., Monié, P., Jolivet, L., Robin, C., & Booth-Rea, G. (2005). Exhumation, doming and slab retreat in the Betic Cordillera (SE Spain): In situ $^{40}\text{Ar}/^{39}\text{Ar}$ ages and P–T–t paths for the Nevado-Filabride complex. *Journal of Metamorphic Geology*, 23(5), 357–381. <https://doi.org/10.1111/j.1525-1314.2005.00581.x>

- Augier, R., Booth-Rea, G., Agard, P., Martínez-Martínez, J. M., Jolivet, L., & Azañón, J. M. (2005). Exhumation constraints for the lower Nevado-Filabride complex (Betic Cordillera, SE Spain): A Raman thermometry and Tweek multiequilibrium thermobarometry approach. *Bulletin de la Societe Geologique de France*, 176(5), 403–416. <https://doi.org/10.2113/176.5.403>
- Augier, R., Jolivet, L., Do Couto, D., & Negro, F. (2013). From ductile to brittle, late- to post-orogenic evolution of the Betic Cordillera: Structural insights from the northeastern Internal zones. *Bulletin de la Societe Geologique de France*, 184(4–5), 405–425.
- Augier, R., Jolivet, L., & Robin, C. (2005). Late Orogenic doming in the eastern Betic Cordilleras: Final exhumation of the Nevado-Filabride complex and its relation to basin Genesis. *Tectonics*, 24(4). <https://doi.org/10.1029/2004TC001687>
- Azañón, J., García-Dueñas, V., & Goffé, B. (1998). Exhumation of high-pressure metapelites and coeval crustal extension in the Alpujarride complex (Betic Cordillera). *Tectonophysics*, 285(3–4), 231–252. [https://doi.org/10.1016/S0040-1951\(97\)00273-4](https://doi.org/10.1016/S0040-1951(97)00273-4)
- Azañón, J. M., Crespo-blanc, A., & García-Dueñas, V. (1997). Continental collision, crustal thinning and nappe forming during the pre-Miocene evolution of the Alpujarride Complex (Alboran Domain, Betics). *Journal of Structural Geology*, 19(8), 1055–1071. [https://doi.org/10.1016/S0191-8141\(97\)00031-X](https://doi.org/10.1016/S0191-8141(97)00031-X)
- Balanyá, J., & García-Dueñas, V. (1987). Les directions structurales dans le Domaine d'Alborán de part et d'autre du Déroit de Gibraltar. *Comptes rendus de l'Académie des sciences. Série 2, Mécanique, Physique, Chimie, Sciences de l'univers, Sciences de la Terre*, 304(15), 929–932.
- Behr, W., & Platt, J. (2012). Kinematic and thermal evolution during two-stage exhumation of a Mediterranean subduction complex. *Tectonics*, 31(4).
- Bessière, E. (2019). *Évolution géodynamique des Zones Internes des Cordillères Bétiques (Andalousie, Espagne): Apports d'une étude pluridisciplinaire du Complexe Alpujarride*. Université d'Orléans.
- Bessière, E., Jolivet, L., Augier, R., Scaillet, S., Précigout, J., Azañón, J.-M., et al. (2021). Lateral variations of pressure-temperature evolution in non-cylindrical orogens and 3-D subduction dynamics: The Betic-Rif Cordillera example. *BSGF-Earth Sciences Bulletin*, 192(1), 8. <https://doi.org/10.1051/bsgf/2021007>
- Bessière, E., Scaillet, S., Augier, R., Jolivet, L., Miguel Azañón, J., Booth-Rea, G., et al. (2022). ⁴⁰Ar/³⁹Ar age constraints on HP/LT metamorphism in extensively overprinted units: The example of the Alpujarride subduction complex (Betic Cordillera, Spain). *Tectonics*, 41(2), e2021TC006889.
- Booth-Rea, G., Azañón, J. M., & García-Dueñas, V. c. (2004). Extensional tectonics in the northeastern Betics (SE Spain): Case study of extension in a multilayered upper crust with contrasting rheologies. *Journal of Structural Geology*, 26(11), 2039–2058. <https://doi.org/10.1016/j.jsg.2004.04.005>
- Booth-Rea, G., Azañón, J. M., Goffé, B., Vidal, O., & Martínez-Martínez, J. M. (2002). High-pressure, low-temperature metamorphism in Alpujarride units of southeastern Betics (Spain). *Comptes Rendus Geoscience*, 334(11), 857–865. [https://doi.org/10.1016/S1631-0713\(02\)01787-X](https://doi.org/10.1016/S1631-0713(02)01787-X)
- Booth-Rea, G., Azañón, J. M., Martínez-Martínez, J. M., Vidal, O., & García-Dueñas, V. (2005). Contrasting structural and P-T evolution of tectonic units in the southeastern Betics: Key for understanding the exhumation of the Alboran Domain HP/LT crustal rocks (western Mediterranean). *Tectonics*, 24(2).
- Booth-Rea, G., Bardají Azcárate, T., & Santos-García, J. A. (2009a). *Mapa Geológico MAGNA de Águilas (997)*. MAGNA de Murcia, IGME.
- Booth-Rea, G., Bardají Azcárate, T., & Santos-García, J. A. (2009b). *Mapa Geológico MAGNA de Puerto Lumbreras (975)*. MAGNA de Murcia, IGME.
- Booth-Rea, G., Martínez-Martínez, J., & Giaconia, F. (2015). Continental subduction, intracrustal shortening, and coeval upper-crustal extension: PT evolution of subducted south Iberian paleomargin metapelites (Betics, SE Spain). *Tectonophysics*, 663, 122–139. <https://doi.org/10.1016/j.tecto.2015.08.036>
- Booth-Rea, G., Ranero, C. R., Martínez-Martínez, J. M., & Grevemeyer, I. (2007). Crustal types and tertiary tectonic evolution of the Alborán sea, Western Mediterranean. *Geochemistry, Geophysics, Geosystems*, 8(10). <https://doi.org/10.1029/2007GC001639>
- Bouillin, J.-P., Durand-Delga, M., & Olivier, P. (1986). Betic-rifian and Tyrrhenian arcs: Distinctive features, genesis and development stages. in *Developments in geotectonics* (pp. 281–304). Elsevier.
- Brun, J.-P. (1983). L'origine des domes gneissiques; modeles et tests. *Bulletin de la Societe Geologique de France*, 7(2), 219–228. <https://doi.org/10.2113/gssgfbull.S7-XXV.2.219>
- Chemenda, A., Matte, P., & Sokolov, V. (1997). A model of Palaeozoic obduction and exhumation of high-pressure/low-temperature rocks in the southern Urals. *Tectonophysics*, 276(1–4), 217–227. [https://doi.org/10.1016/S0040-1951\(97\)00057-7](https://doi.org/10.1016/S0040-1951(97)00057-7)
- Chemenda, A. I., Mattauer, M., & Bokun, A. N. (1996). Continental subduction and a mechanism for exhumation of high-pressure metamorphic rocks: New modelling and field data from Oman. *Earth and Planetary Science Letters*, 143(1–4), 173–182.
- Chertova, M., Spakman, W., Geenen, T., Van Den Berg, A., & Van Hinsbergen, D. (2014). Underpinning tectonic reconstructions of the western Mediterranean region with dynamic slab evolution from 3-D numerical modeling. *Journal of Geophysical Research: Solid Earth*, 119(7), 5876–5902. <https://doi.org/10.1002/2014JB011150>
- Comas, M., Platt, J., Soto, J., & Watts, A. (1999). 44. The origin and tectonic history of the Alboran basin: Insights from Leg 161 results. In Paper presented at Proceedings of the Ocean Drilling Program Scientific Results.
- de Jong, K. (2003). Very fast exhumation of high-pressure metamorphic rocks with excess ⁴⁰Ar and inherited ⁸⁷Sr, Betic Cordilleras, southern Spain. *Lithos*, 70(3–4), 91–110. [https://doi.org/10.1016/S0024-4937\(03\)00094-X](https://doi.org/10.1016/S0024-4937(03)00094-X)
- De Jong, K., Féraud, G., Ruffet, G., Amouric, M., & Wijbrans, J. (2001). Excess argon incorporation in phengite of the Mulhacén Complex: Submicroscopic illitization and fluid ingress during late Miocene extension in the Betic Zone, south-eastern Spain. *Chemical Geology*, 178(1–4), 159–195.
- de Jong, K., Wijbrans, J. R., & Féraud, G. (1992). Repeated thermal resetting of phengites in the Mulhacén Complex (Betic Zone, southeastern Spain) shown by ⁴⁰Ar/³⁹Ar step heating and single grain laser probe dating. *Earth and Planetary Science Letters*, 110(1–4), 173–191. [https://doi.org/10.1016/0012-821X\(92\)90047-Y](https://doi.org/10.1016/0012-821X(92)90047-Y)
- Faccenna, C., Piromallo, C., Crespo-Blanc, A., Jolivet, L., & Rossetti, F. (2004). Lateral slab deformation and the origin of the Western Mediterranean arcs. *Tectonics*, 23(1). <https://doi.org/10.1029/2002tc001488>
- García-Dueñas, V., Balanyá, J., & Martínez-Martínez, J. (1992). Miocene extensional detachments in the outcropping basement of the northern Alboran basin (Betics) and their tectonic implications. *Geo-Marine Letters*, 12(2–3), 88–95. <https://doi.org/10.1007/BF02084917>
- García-Dueñas, V., Martínez Martínez, J., Orozco, M., & Soto, J. (1988). Plis-nappes, cisaillements syn-à post-métamorphiques et cisaillement ductiles-fragiles en distension dans les Nevado-Filábrides (Cordillères Bétiques, Espagne). *Comptes rendus de l'Académie des sciences. Série 2, Mécanique, Physique, Chimie, Sciences de l'univers, Sciences de la Terre*, 307(11), 1389–1395.
- García Monzón, G., Kampschuur, W., & Verburg, J. (1974). *Mapa geológico de Espana, Hoja 1031, Sorbas*. Madrid: Instituto Geologico y Minero de Espana (IGME), Ministerio de Industria y Energía. Scale 1:50,000.

- Goffé, B., Michard, A., García-Duenas, V., Gonzalez-Lodeiro, F., Monie, P., Campos, J., et al. (1989). First evidence of high-pressure, low-temperature metamorphism in the Alpujarride nappes, Betic Cordilleras (SE Spain). *European Journal of Mineralogy*, *1*(1), 139–142. <https://doi.org/10.1127/ejm/01/1/0139>
- Goffé, B., Michard, A., Kienast, J. R., & Le Mer, O. (1988). A case of obduction-related high-pressure, low-temperature metamorphism in upper crustal nappes, Arabian continental margin, Oman: PT paths and kinematic interpretation. *Tectonophysics*, *151*(1–4), 363–386. [https://doi.org/10.1016/0040-1951\(88\)90253-3](https://doi.org/10.1016/0040-1951(88)90253-3)
- Gomez-Pugnaire, M. T., & Munoz, M. (1991). Al-Rich xenoliths in the Nevado-Filábride metabasites: Evidence for a continental setting of this basic magmatism in the Betic Cordilleras (SE Spain). *European Journal of Mineralogy*, *3*(1), 193–198. <https://doi.org/10.1127/ejm/3/1/0193>
- Hacker, B. R., Ratschbacher, L., Webb, L., McWilliams, M. O., Ireland, T., Calvert, A., et al. (2000). Exhumation of ultrahigh-pressure continental crust in east central China: Late Triassic–Early Jurassic tectonic unroofing. *Journal of Geophysical Research*, *105*(B6), 13339–13364. <https://doi.org/10.1029/2000JB900039>
- Handy, M. R., Schmid, S. M., Bousquet, R., Kissling, E., & Bernoulli, D. (2010). Reconciling plate-tectonic reconstructions of Alpine Tethys with the geological–geophysical record of spreading and subduction in the Alps. *Earth-Science Reviews*, *102*(3–4), 121–158. <https://doi.org/10.1016/j.earscirev.2010.06.002>
- Harrison, T. M., Célérier, J., Aikman, A. B., Hermann, J., & Heizler, M. T. (2009). Diffusion of ^{40}Ar in muscovite. *Geochimica et Cosmochimica Acta*, *73*(4), 1039–1051. <https://doi.org/10.1016/j.gca.2008.09.038>
- Herwegh, M., Berger, A., Baumberger, R., Wehrens, P., & Kissling, E. (2017). Large-scale crustal-block-extrusion during late Alpine collision. *Scientific Reports*, *7*(1), 413. <https://doi.org/10.1038/s41598-017-00440-0>
- Jabaloy-Sánchez, A., Talavera, C., Gómez-Pugnaire, M. T., López-Sánchez-Vizcaíno, V., Vázquez-Vílchez, M., Rodríguez-Peces, M. J., & Evans, N. J. (2018). U–Pb ages of detrital zircons from the internal Betics: A key to deciphering paleogeographic provenance and tectono-stratigraphic evolution. *Lithos*, *318*, 244–266. <https://doi.org/10.1016/j.lithos.2018.07.026>
- Jabaloy-Sánchez, A., Talavera, C., Rodríguez-Peces, M. J., Vázquez-Vílchez, M., & Evans, N. J. (2021). U–Pb geochronology of detrital and igneous zircon grains from the Águilas Arc in the internal Betics (SE Spain): Implications for Carboniferous–Permian paleogeography of Pangea. *Gondwana Research*, *90*, 135–158. <https://doi.org/10.1016/j.gr.2020.10.013>
- Johnson, C. (1997). Resolving denudational histories in orogenic belts with apatite fission-track thermochronology and structural data: An example from southern Spain. *Geology*, *25*(7), 623–626. [https://doi.org/10.1130/0091-7613\(1997\)025\(0623:Rdhiob\)2.3.Co;2](https://doi.org/10.1130/0091-7613(1997)025(0623:Rdhiob)2.3.Co;2)
- Jolivet, L., & Faccenna, C. (2000). Mediterranean extension and the Africa–Eurasia collision. *Tectonics*, *19*(6), 1095–1106. <https://doi.org/10.1029/2000TC900018>
- Jolivet, L., Lecomte, E., Huet, B., Denèle, Y., Lacombe, O., Labrousse, L., et al. (2010). The north cycladic detachment system. *Earth and Planetary Science Letters*, *289*(1–2), 87–104. <https://doi.org/10.1016/j.epsl.2009.10.032>
- Jolivet, L., Menant, A., Roche, V., Le Pourhiet, L., Maillard, A., Augier, R., et al. (2021). Transfer zones in Mediterranean back-arc regions and tear faults. *BSGF–Earth Sciences Bulletin*, *192*(1), 11. <https://doi.org/10.1051/bsgf/2021006>
- Kirchner, K. L., Behr, W. M., Loewy, S., & Stockli, D. F. (2016). Early Miocene subduction in the western Mediterranean: Constraints from Rb–Sr multiminerall isochron geochronology. *Geochemistry, Geophysics, Geosystems*, *17*(5), 1842–1860. <https://doi.org/10.1002/2015GC006208>
- Koppers, A. A. (2002). ArArCALC—Software for $^{40}\text{Ar}/^{39}\text{Ar}$ age calculations. *Computers & Geosciences*, *28*(5), 605–619. [https://doi.org/10.1016/S0098-3004\(01\)00095-4](https://doi.org/10.1016/S0098-3004(01)00095-4)
- Kuiper, K., Deino, A., Hilgen, F., Krijgsman, W., Renne, P., & Wijbrans, J. R. (2008). Synchronizing rock clocks of Earth history. *Science*, *320*(5875), 500–504. <https://doi.org/10.1126/science.1154339>
- Laborda-López, C., Marchesi, C., Sánchez-Vizcaíno, V. L., Gómez-Pugnaire, M. T., Dale, C. W., Jabaloy-Sánchez, A., et al. (2020). Geochemical evolution of rodingites during subduction: Insights from Cerro del Almirez (southern Spain). *Lithos*, *370*, 105639. <https://doi.org/10.1016/j.lithos.2020.105639>
- Li, B., & Massonne, H. J. (2018). Two tertiary metamorphic events recognized in high-pressure metapelites of the Nevado-Filábride Complex (Betic Cordillera, S Spain). *Journal of Metamorphic Geology*, *36*(5), 603–630. <https://doi.org/10.1111/jmg.12312>
- Lips, A., White, S., & Wijbrans, J. (1998). $^{40}\text{Ar}/^{39}\text{Ar}$ laserprobe direct dating of discrete deformational events: A continuous record of early Alpine tectonics in the Pelagonian zone, NW Aegean area, Greece. *Tectonophysics*, *298*(1), 133–153. [https://doi.org/10.1016/S0040-1951\(98\)00181-4](https://doi.org/10.1016/S0040-1951(98)00181-4)
- Lister, G., & Forster, M. (2016). White mica $^{40}\text{Ar}/^{39}\text{Ar}$ age spectra and the timing of multiple episodes of high-P metamorphic mineral growth in the Cycladic eclogite–blueschist belt, Syros, Aegean Sea, Greece. *Journal of Metamorphic Geology*, *34*(5), 401–421. <https://doi.org/10.1111/jmg.12178>
- Loneragan, L., & Johnson, C. (2002). Reconstructing orogenic exhumation histories using synorogenic detrital zircons and apatites: An example from the Betic Cordillera, SE Spain. *Basin Research*, *10*(3), 353–364. <https://doi.org/10.1046/j.1365-2117.1998.00071.x>
- Loneragan, L., & White, N. (1997). Origin of the Betic-Rif mountain belt. *Tectonics*, *16*(3), 504–522. <https://doi.org/10.1029/96TC03937>
- Marrone, S., Monié, P., Rossetti, F., Aldega, L., Bouybaouene, M., Charpentier, D., et al. (2021). Timing of Alpine orogeny and postorogenic extension in the Alboran domain, Inner Rif Chain, Morocco. *Tectonics*, *40*(7), e2021TC006707. <https://doi.org/10.1029/2021TC006707>
- Marrone, S., Monié, P., Rossetti, F., Lucci, F., Theye, T., Bouybaouene, M. L., & Zaghoul, M. N. (2021). The pressure–temperature–time–deformation history of the Beni Mzala unit (Upper Sebides, Rif belt, Morocco): Refining the Alpine tectono-metamorphic evolution of the Alboran Domain of the western Mediterranean. *Journal of Metamorphic Geology*, *39*(5), 591–615. <https://doi.org/10.1111/jmg.12587>
- Martínez Martínez, J. (1984). Las sucesiones Nevado-Filábrides en la Sierra de los Filabres y Sierra Nevada. *Correlaciones*.
- Martínez-Martínez, J., & Azañón, J. (1997). Mode of extensional tectonics in the southeastern Betics (SE Spain): Implications for the tectonic evolution of the peri-Alborán orogenic system. *Tectonics*, *16*(2), 205–225. <https://doi.org/10.1029/97TC00157>
- Martínez-Martínez, J., Soto, J., & Balanyá, J. (2002). Orthogonal folding of extensional detachments: Structure and origin of the Sierra Nevada elongated dome (Betics, SE Spain). *Tectonics*, *21*(3), 3–1–3–20. <https://doi.org/10.1029/2001TC001283>
- Martínez-Martínez, J., Torres-Ruiz, J., Pesquera, A., & Gil-Crespo, P. (2010). Geological relationships and U–Pb zircon and $^{40}\text{Ar}/^{39}\text{Ar}$ tourmaline geochronology of gneisses and tourmalinites from the Nevado-Filábride complex (western Sierra Nevada, Spain): Tectonic implications. *Lithos*, *119*(3–4), 238–250. <https://doi.org/10.1016/j.lithos.2010.07.002>
- Martínez Martínez, J. M. (1986). Evolución tectónico-metamórfica del Complejo Nevado-Filábride en el sector de unión entre Sierra Nevada y Sierra de los Filabres (Cordilleras Béticas).
- Massonne, H., Coleman, R., & Wang, X. (1995). *Experimental and petrogenetic study of UHPM* (pp. 33–95). Ultrahigh pressure metamorphism.
- Massonne, H.-J., & Schreyer, W. (1987). Phengite geobarometry based on the limiting assemblage with K-feldspar, phlogopite, and quartz. *Contributions to Mineralogy and Petrology*, *96*(2), 212–224. <https://doi.org/10.1007/Bf00375235>
- Matenco, L., & Schmid, S. (1999). Exhumation of the Danubian nappes system (South Carpathians) during the Early Tertiary: Inferences from kinematic and paleostress analysis at the Getic/Danubian nappes contact. *Tectonophysics*, *314*(4), 401–422. [https://doi.org/10.1016/S0040-1951\(99\)00221-8](https://doi.org/10.1016/S0040-1951(99)00221-8)

- Menzel, M. D., Garrido, C. J., López Sánchez-Vizcaíno, V., Hidas, K., & Marchesi, C. (2019). Subduction metamorphism of serpentinite-hosted carbonates beyond antigorite-serpentinite dehydration (Nevado-Filábride Complex, Spain). *Journal of Metamorphic Geology*, 37(5), 681–715. <https://doi.org/10.1111/jmg.12481>
- Monié, P., Galindo-Zaldívar, J., Lodeiro, F. G., Goffe, B., & Jabaloy, A. (1991). ⁴⁰Ar/³⁹Ar geochronology of Alpine tectonism in the Betic Cordilleras (southern Spain). *Journal of the Geological Society*, 148(2), 289–297. <https://doi.org/10.1144/gsjgs.148.2.0289>
- Monié, P., Torres-Roldán, R., & García-Casco, A. (1994). Cooling and exhumation of the Western Betic Cordilleras, ⁴⁰Ar/³⁹Ar thermochronological constraints on a collapsed terrane. *Tectonophysics*, 238(1–4), 353–379. [https://doi.org/10.1016/0040-1951\(94\)90064-7](https://doi.org/10.1016/0040-1951(94)90064-7)
- Moragues, L., Ruano, P., Azañón, J. M., Garrido, C. J., Hidas, K., & Booth Rea, G. (2021). Two Cenozoic extensional phases in Mallorca and their bearing on the geodynamic evolution of the western Mediterranean. *Tectonics*, 40(11), e2021TC006868. <https://doi.org/10.1029/2021TC006868>
- Morten, L., Bargossi, G., Martínez, J. M., Puga, E., & de Federico, A. D. (1987). Metagabbro and associated eclogites in the Lubrin area, Nevado-Filábride Complex, Spain. *Journal of Metamorphic Geology*, 5(2), 155–174. <https://doi.org/10.1111/j.1525-1314.1987.tb00377.x>
- Ortí, F., Pérez-López, A., & Salvany, J. M. (2017). Triassic evaporites of Iberia: Sedimentological and palaeogeographical implications for the western Neotethys evolution during the middle Triassic–Earliest Jurassic. *Palaeogeography, Palaeoclimatology, Palaeoecology*, 471, 157–180. <https://doi.org/10.1016/j.palaeo.2017.01.025>
- Padrón-Navarta, J. A., Hermann, J., Garrido, C. J., Sánchez-Vizcaíno, V. L., & Gómez-Pugnaire, M. T. (2010). An experimental investigation of antigorite dehydration in natural silica-enriched serpentinite. *Contributions to Mineralogy and Petrology*, 159(1), 25. <https://doi.org/10.1007/s00410-009-0414-5>
- Pedreira, A., Galindo-Zaldívar, J., Ruiz-Constán, A., Duque, C., Marín-Lechado, C., & Serrano, I. (2009). Recent large fold nucleation in the upper crust: Insight from gravity, magnetic, magnetotelluric and seismicity data (Sierra de Los Filabres–Sierra de Las Estancias, Internal Zones, Betic Cordillera). *Tectonophysics*, 463(1–4), 145–160. <https://doi.org/10.1016/j.tecto.2008.09.037>
- Pedreira, A., Ruiz-Constán, A., García-Senz, J., Azor, A., Marín-Lechado, C., Ayala, C., et al. (2020). Evolution of the South-Iberian paleomargin: From hyperextension to continental subduction. *Journal of Structural Geology*, 138, 104122. <https://doi.org/10.1016/j.jsg.2020.104122>
- Platt, J. (1986). Dynamics of orogenic wedges and the uplift of high-pressure metamorphic rocks. *The Geological Society of America Bulletin*, 97(9), 1037–1053. [https://doi.org/10.1130/0016-7606\(1986\)97<1037:Doowat>2.0.Co;2](https://doi.org/10.1130/0016-7606(1986)97<1037:Doowat>2.0.Co;2)
- Platt, J., Allerton, S., Kirker, A., Mandeville, C., Mayfield, A., Platzman, E., & Rimi, A. (2003). The ultimate arc: Differential displacement, oroclinal bending, and vertical axis rotation in the External Betic-Rif arc. *Tectonics*, 22(3). <https://doi.org/10.1029/2001TC001321>
- Platt, J., Behrmann, J., Martínez, J.-M., & Vissers, R. (1984). A zone of mylonite and related ductile deformation beneath the Alpujarride Nappe Complex, Betic Cordilleras, S. Spain. *Geologische Rundschau*, 73(2), 773–785. <https://doi.org/10.1007/BF01824981>
- Platt, J., Kelley, S., Carter, A., & Orozco, M. (2005). Timing of tectonic events in the Alpujarride complex, Betic Cordillera, southern Spain. *Journal of the Geological Society*, 162(3), 451–462. <https://doi.org/10.1144/0016-764903-039>
- Platt, J., & Vissers, R. (1980). Extensional structures in anisotropic rocks. *Journal of Structural Geology*, 2(4), 397–410. [https://doi.org/10.1016/0191-8141\(80\)90002-4](https://doi.org/10.1016/0191-8141(80)90002-4)
- Platt, J., Whitehouse, M., Kelley, S., Carter, A., & Hollick, L. (2003). Simultaneous extensional exhumation across the Alboran Basin: Implications for the causes of late orogenic extension. *Geology*, 31(3), 251–254. [https://doi.org/10.1130/0091-7613\(2003\)031<0251:Seeata>2.0.Co;2](https://doi.org/10.1130/0091-7613(2003)031<0251:Seeata>2.0.Co;2)
- Platt, J. P., Anczkiewicz, R., Soto, J.-I., Kelley, S. P., & Thirlwall, M. (2006). Early Miocene continental subduction and rapid exhumation in the western Mediterranean. *Geology*, 34(11), 981–984. <https://doi.org/10.1130/G22801a.1>
- Porkoláb, K., Duret, T., Yamato, P., Auzemery, A., & Willingshofer, E. (2021). Extrusion of subducted crust explains the emplacement of far-travelled ophiolites. *Nature Communications*, 12(1), 1–11. <https://doi.org/10.1038/s41467-021-21866-1>
- Porkoláb, K., Willingshofer, E., Sokoutis, D., Creton, I., Kostopoulos, D., & Wijbrans, J. (2019). Cretaceous-paleogene tectonics of the Pelagonian zone: Inferences from Skopelos island (Greece). *Tectonics*, 38(6), 1946–1973. <https://doi.org/10.1029/2018TC005331>
- Pourteau, A., Sudo, M., Candan, O., Lanari, P., Vidal, O., & Oberhänsli, R. (2013). Neotethys closure history of Anatolia: Insights from ⁴⁰Ar–³⁹Ar geochronology and P–T estimation in high-pressure metasedimentary rocks. *Journal of Metamorphic Geology*, 31(6), 585–606. <https://doi.org/10.1111/jmg.12034>
- Puga, E. (2005). *A reappraisal of the Betic Ophiolitic Association: The westernmost relic of the Alpine Tethys Ocean. Deep Seismic Exploration of the Central Mediterranean and Italy* (Vol. 1, pp. 665–704). University of Trieste, Elsevier, Crosta Profonda (CROP).
- Puga, E., De Federico, A. D., & Nieto, J. M. (2002). Tectonostratigraphic subdivision and petrological characterisation of the deepest complexes of the Betic zone: A review. *Geodinamica Acta*, 15(1), 23–43. [https://doi.org/10.1016/S0985-3111\(01\)01077-4](https://doi.org/10.1016/S0985-3111(01)01077-4)
- Puga, E., Díaz de Federico, A., Fanning, M., Nieto, J. M., Rodríguez Martínez-Conde, J. Á., Díaz Puga, M. Á., et al. (2017). The Betic ophiolites and the Mesozoic evolution of the Western Tethys. *Geosciences*, 7(2), 31.
- Puga, E., Fanning, M., de Federico, A. D., Nieto, J. M., Beccaluva, L., Bianchini, G., & Puga, M. A. D. (2011). Petrology, geochemistry and U–Pb geochronology of the Betic ophiolites: Inferences for Pangaea break-up and birth of the westernmost Tethys Ocean. *Lithos*, 124(3–4), 255–272.
- Puga, E., Nieto, J., de Federico, A. D., Bodinier, J. A., & Morten, L. (1999). Petrology and metamorphic evolution of ultramafic rocks and dolerite dykes of the Betic Ophiolitic Association (Mulhacén Complex, SE Spain): Evidence of eo-Alpine subduction following an ocean-floor metasomatic process. *Lithos*, 49(1–4), 23–56.
- Puga, E., Nieto, J. M., & De Federico, A. D. (2000). Contrasting P–T paths in eclogites of the Betic ophiolitic association, Mulhacén complex, southeastern Spain. *The Canadian Mineralogist*, 38(5), 1137–1161. <https://doi.org/10.2113/gscanmin.38.5.1137>
- Reston, T. J., Leythäuser, T., Booth-Rea, G., Sawyer, D., Klaeschen, D., & Long, C. (2007). Movement along a low-angle normal fault: The S reflector west of Spain. *Geochemistry, Geophysics, Geosystems*, 8(6).
- Rey, P. F., Teyssier, C., Kruckenberg, S. C., & Whitney, D. L. (2011). Viscous collision in channel explains double domes in metamorphic core complexes. *Geology*, 39(4), 387–390.
- Romagny, A., Jolivet, L., Menant, A., Bessière, E., Maillard, A., Canva, A., et al. (2020). Detailed tectonic reconstructions of the Western Mediterranean region for the last 35 Ma, insights on driving mechanisms [Reconstructions détaillées de la Méditerranée occidentale depuis 35 Ma, implications en terme de mécanismes moteur]. *Bulletin de la Société Géologique de France*, 191(1).
- Rosenbaum, G., Lister, G. S., & Duboz, C. (2002). Reconstruction of the tectonic evolution of the western Mediterranean since the Oligocene. *Journal of the Virtual Explorer*, 8(January), 107–130.
- Rossetti, F., Faccenna, C., & Crespo-Blanc, A. (2005). Structural and kinematic constraints to the exhumation of the Alpujarride Complex (Central Betic Cordillera, Spain). *Journal of Structural Geology*, 27(2), 199–216.
- Ruiz-Cruz, M. D., de Galdeano, C. S., & Santamaría, A. (2015). Petrology and thermobarometric estimates for metasediments, orthogneisses, and eclogites from the Nevado-Filábride complex in the western Sierra Nevada (Betic Cordillera, Spain). *The Canadian Mineralogist*, 53(6), 1083–1107.
- Sánchez-Vizcaíno, V. L., Rubatto, D., Gómez-Pugnaire, M. T., Trommsdorff, V., & Müntener, O. (2001). Middle Miocene high-pressure metamorphism and fast exhumation of the Nevado-Filábride Complex, SE Spain. *Terra Nova*, 13(5), 327–332.

- Santamaría-López, Á., Lanari, P., & de Galdeano, C. S. (2019). Deciphering the tectono-metamorphic evolution of the Nevado-Filábride complex (Betic Cordillera, Spain)—A petrochronological study. *Tectonophysics*, *767*, 128158.
- Scharf, A., Handy, M., Favaro, S., Schmid, S. M., & Bertrand, A. (2013). Modes of orogen-parallel stretching and extensional exhumation in response to microplate indentation and roll-back subduction (Tauern Window, Eastern Alps). *International Journal of Earth Sciences*, *102*(6), 1627–1654.
- Schmid, S. M., Bernoulli, D., Fügenschuh, B., Matenco, L., Schefer, S., Schuster, R., et al. (2008). The Alpine-Carpathian-Dinaridic orogenic system: Correlation and evolution of tectonic units. *Swiss Journal of Geosciences*, *101*(1), 139–183.
- Schneider, B., Kuiper, K., Postma, O., & Wijbrans, J. (2009). $^{40}\text{Ar}/^{39}\text{Ar}$ geochronology using a quadrupole mass spectrometer. *Quaternary Geochronology*, *4*(6), 508–516.
- Simon, O. (1987). On the Triassic of the Betic Cordilleras (Southern Spain). *Cuadernos de Geología Iberica*, *11*, 385–402.
- Simpson, C., & Schmid, S. M. (1983). An evaluation of criteria to deduce the sense of movement in sheared rocks. *The Geological Society of America Bulletin*, *94*(11), 1281–1288.
- Spakman, W., Chertova, M. V., van den Berg, A., & van Hinsbergen, D. J. (2018). Puzzling features of western Mediterranean tectonics explained by slab dragging. *Nature Geoscience*, *11*(3), 211–216.
- Tendero, J., Martín-Algarra, A., Puga, E., & Díaz de Federico, A. (1993). Lithostratigraphie des métasédiments de l'association ophiolitique Nevado-Filábride (SE Espagne) et mise en évidence d'objets ankéritiques évoquant des foraminifères planctoniques du Crétacé: Conséquences paléogéographiques. *Comptes rendus de l'Académie des sciences. Série 2, Mécanique, Physique, Chimie, Sciences de l'univers, Sciences de la Terre*, *316*(8), 1115–1122.
- Uunk, B., Brouwer, F., ter Voorde, M., & Wijbrans, J. (2018). Understanding phengite argon closure using single grain fusion age distributions in the Cycladic Blueschist Unit on Syros, Greece. *Earth and Planetary Science Letters*, *484*, 192–203.
- van Hinsbergen, D. J., Maffione, M., Plunder, A., Kaymakci, N., Ganerød, M., Hendriks, B. W., et al. (2016). Tectonic evolution and paleogeography of the Kirşehir block and the Central Anatolian ophiolites, Turkey. *Tectonics*, *35*(4), 983–1014.
- van Hinsbergen, D. J., Torsvik, T. H., Schmid, S. M., Matenco, L. C., Maffione, M., Vissers, R. L., et al. (2020). Orogenic architecture of the Mediterranean region and kinematic reconstruction of its tectonic evolution since the Triassic. *Gondwana Research*, *81*, 79–229.
- van Hinsbergen, D. J., Vissers, R. L., & Spakman, W. (2014). Origin and consequences of western Mediterranean subduction, rollback, and slab segmentation. *Tectonics*, *33*(4), 393–419.
- Vázquez, M., Jabaloy, A., Barbero, L., & Stuart, F. M. (2011). Deciphering tectonic- and erosion-driven exhumation of the Nevado-Filábride Complex (Betic Cordillera, Southern Spain) by low temperature thermochronology. *Terra Nova*, *23*(4), 257–263.
- Vergés, J., & Fernández, M. (2012). Tethys–Atlantic interaction along the Iberia–Africa plate boundary: The Betic–Rif orogenic system. *Tectonophysics*, *579*, 144–172.
- Villa, I. (1998). Isotopic closure. *Terra Nova*, *10*(1), 42–47.
- Vissers, R. (2012). Extension in a convergent tectonic setting: A lithospheric view on the Alboran system of SW Europe. *Geologica Belgica*, *15*(1–2), 53.
- Vissers, R., Platt, J., & Van der Wal, D. (1995). Late orogenic extension of the Betic Cordillera and the Alboran domain: A lithospheric view. *Tectonics*, *14*(4), 786–803.
- Warren, C. J., Kelley, S. P., Sherlock, S. C., & McDonald, C. S. (2012). Metamorphic rocks seek meaningful cooling rate: Interpreting $^{40}\text{Ar}/^{39}\text{Ar}$ ages in an exhumed ultra-high pressure terrane. *Lithos*, *155*, 30–48.
- Wijbrans, J., Pringle, M., Koppers, A., & Scheveers, R. (1995). Argon geochronology of small samples using the Vulkaan argon laserprobe. Paper presented at Proceedings of the Royal Netherlands Academy of Arts and Sciences.
- Wijbrans, J. R., & McDougall, I. (1986). $^{40}\text{Ar}/^{39}\text{Ar}$ dating of white micas from an Alpine high-pressure metamorphic belt on Naxos (Greece): The resetting of the argon isotopic system. *Contributions to Mineralogy and Petrology*, *93*(2), 187–194.
- Wijbrans, J. R., Schliestedt, M., & York, D. (1990). Single grain argon laser probe dating of phengites from the blueschist to greenschist transition on Sifnos (Cyclades, Greece). *Contributions to Mineralogy and Petrology*, *104*(5), 582–593.
- Yılmaz, P., & Maxwell, J. (1984). An example of an obduction melange: The Alakir Çay unit, Antalya Complex, southwest Turkey. *Melanges: Their nature, origin, and significance: Geological Society of America Special Paper*, *198*, 139–152.